Article

Immunity

CD4+ T cell-mediated recognition of a conserved cholesterol-dependent cytolysin epitope generates broad antibacterial immunity

Graphical abstract

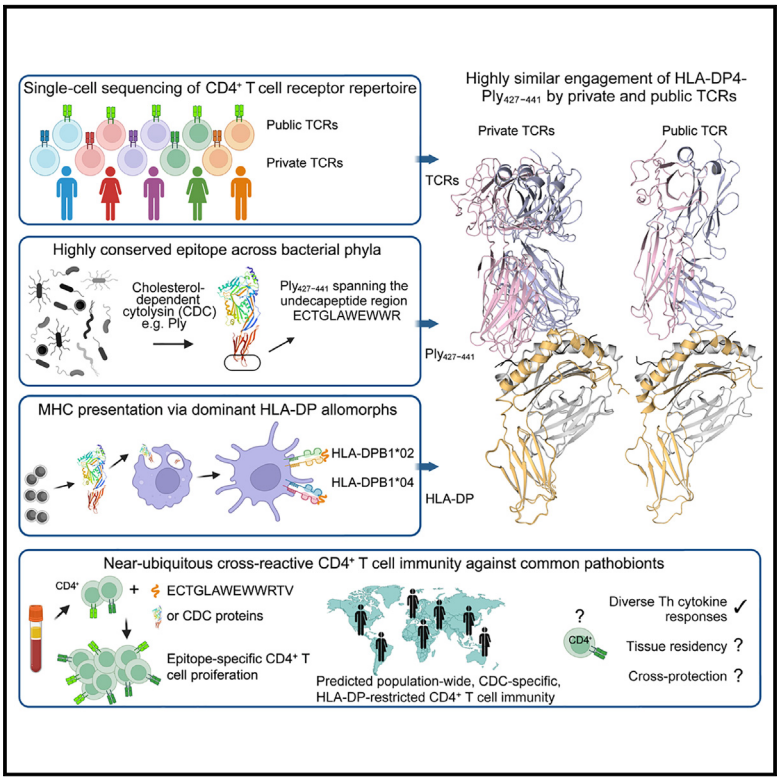

Highlights

- CD4+ T cells recognize a conserved bacterial epitope from pneumolysin ($Ply_{427–441}$)
- $Ply_{427–441}$ is presented by the globally abundant HLA allomorphs DPB1*02 and DPB1*04
- $Ply_{427–441}$ is recognized by architecturally diverse TCRs in the context of HLA-DPB1*04
- Cross-recognition of related epitopes generates *trans*-phyla bacterial immunity

Authors

Lisa Ciacchi, Martijn D.B. van de Garde, Kristin Ladell, ..., David A. Price, Jamie Rossjohn, Cécile A.C.M. van Els

Correspondence

priced6@cardiff.ac.uk (D.A.P.), jamie.rossjohn@monash.edu (J.R.), cecile.van.els@rivm.nl (C.A.C.M.v.E.)

In brief

CD4+ T cell-mediated immunity protects against infection with *Streptococcus pneumoniae* (pneumococcus), but the relevant antigens have not been identified previously. Ciacchi et al. show that near-ubiquitous CD4+ T cell reactivity against a conserved epitope from the pneumococcal cholesterol-dependent cytolysin (CDC) pneumolysin generates *trans*-phyla immunity against divergent bacterial pathogens encoding CDCs.

Ciacchi et al., 2023, Immunity *56*, 1082–1097
May 9, 2023
https://doi.org/10.1016/j.immuni.2023.03.020

CellPress

CellPress
OPEN ACCESS

Immunity

Article

CD4+ T cell-mediated recognition of a conserved cholesterol-dependent cytolysin epitope generates broad antibacterial immunity

Lisa Ciacchi,[1,6] Martijn D.B. van de Garde,[2,6] Kristin Ladell,[3,6] Carine Farenc,[1] Martien C.M. Poelen,[2] Kelly L. Miners,[3] Carmen Llerena,[1] Hugh H. Reid,[1] Jan Petersen,[1] David A. Price,[3,4,*] Jamie Rossjohn,[1,3,4,*] and Cécile A.C.M. van Els[2,5,7,*]

[1]Infection and Immunity Program, Department of Biochemistry and Molecular Biology, Monash Biomedicine Discovery Institute, Monash University, Clayton, VIC 3800, Australia

[2]Centre for Infectious Disease Control, National Institute for Public Health and the Environment (RIVM), Bilthoven, Utrecht 3721MA, the Netherlands

[3]Division of Infection and Immunity, Cardiff University School of Medicine, University Hospital of Wales, Cardiff CF14 4XN, UK

[4]Systems Immunity Research Institute, Cardiff University School of Medicine, University Hospital of Wales, Cardiff CF14 4XN, UK

[5]Infectious Diseases and Immunology, Department of Biomolecular Health Sciences, Faculty of Veterinary Medicine, Utrecht University, Utrecht 3584CL, the Netherlands

[6]These authors contributed equally

[7]Lead contact

*Correspondence: priced6@cardiff.ac.uk (D.A.P.), jamie.rossjohn@monash.edu (J.R.), cecile.van.els@rivm.nl (C.A.C.M.v.E.)

https://doi.org/10.1016/j.immuni.2023.03.020

SUMMARY

CD4+ T cell-mediated immunity against *Streptococcus pneumoniae* (pneumococcus) can protect against recurrent bacterial colonization and invasive pneumococcal diseases (IPDs). Although such immune responses are common, the pertinent antigens have remained elusive. We identified an immunodominant CD4+ T cell epitope derived from pneumolysin (Ply), a member of the bacterial cholesterol-dependent cytolysins (CDCs). This epitope was broadly immunogenic as a consequence of presentation by the pervasive human leukocyte antigen (HLA) allotypes DPB1*02 and DPB1*04 and recognition via architecturally diverse T cell receptors (TCRs). Moreover, the immunogenicity of $Ply_{427–444}$ was underpinned by core residues in the conserved undecapeptide region (ECTGLAWEWWR), enabling cross-recognition of heterologous bacterial pathogens expressing CDCs. Molecular studies further showed that HLA-DP4-$Ply_{427–441}$ was engaged similarly by private and public TCRs. Collectively, these findings reveal the mechanistic determinants of near-global immune focusing on a *trans*-phyla bacterial epitope, which could inform ancillary strategies to combat various life-threatening infectious diseases, including IPDs.

INTRODUCTION

Streptococcus pneumoniae (pneumococcus) is a bacterial pathogen responsible for a high burden of morbidity and mortality worldwide.[1] Pneumococcus causes a variety of illnesses, ranging in severity from acute otitis media and sinusitis to life-threatening conditions such as meningitis, pneumonia, and septicemia, which are collectively known as invasive pneumococcal diseases (IPDs).[2–6] Natural colonization of the nasopharyngeal mucosa is often asymptomatic and occurs commonly during the first year of life, eventually declining with age to carriage rates of <65% in children[7] and <10% in adults.[8,9] Each strain can persist for weeks to months after acquisition, and each colonization event typically elicits adaptive cellular and humoral immunity.[10–13] Antibody responses targeting pneumococcal capsular polysaccharides are highly protective and underpin the efficacy of licensed conjugate vaccines against IPDs.[14,15] However, recent lines of evidence have also indicated an important role for naturally acquired pneumococcal-protein-specific immunity, which could help prevent successive colonization events and various disease manifestations in a serotype-independent manner.[16]

The pneumococcal virulence factor pneumolysin (Ply) has been tested in detoxified form (dPly) as a potential serotype-independent vaccine candidate to protect against IPDs.[17–19] This cytotoxin belongs to a large family of bacterial pore-forming cholesterol-dependent cytolysins (CDCs),[20,21] which bind cholesterol-rich eukaryotic cell membranes via a tryptophan-rich undecapeptide loop (ECTGLAWEWWR)[22–24] and subsequently assemble into transmembrane pores to initiate cell death.[22,25–28] Other roles have also been attributed to CDCs. For example, Ply can interfere with host defense mechanisms[29–31] and elicit antibody responses, which protect against further episodes of pneumococcal colonization.[5,6,32,33]

CD4$^+$ T cell immunity against pneumococcus has been characterized previously in mice. Several immunodominant epitopes have been identified in Ply,[34] and pneumococcus-specific responses with T helper-17 (Th17)-like functionality have been associated with protection.[35–37] Moreover, a key role for CD4$^+$ T cells in the overall immune response against *S. pneumoniae* has been demonstrated in murine models, where increased bacterial loads are observed in the lungs of major histocompatibility complex (MHC) class-II-deficient mice, and reduced pneumococcal colonization is observed in antibody-deficient mice.[6,32,38,39] It has nonetheless remained unclear to what extent these paradigms apply in the context of human immunity, despite the fact that natural colonization events have been shown to induce Ply-specific CD4$^+$ T cells that secrete interleukin-17 (IL-17).[8,40–43]

In this study, we identified a highly immunogenic pneumococcal CD4$^+$ T cell epitope derived from the undecapeptide region of Ply, which is conserved across many other bacterial CDCs.[21] This epitope was targeted by a vast majority of healthy adults as a consequence of presentation by the broadly expressed human leukocyte antigen (HLA) allotypes DPB1*02 and DPB1*04 and immune recognition via a diverse array of public (shared) and private (unique) $\alpha\beta$ T cell receptors (TCRs). Cross-species immune recognition of this communal epitope was further enabled by the featured nature of the antigenic complex, which provided common points of contact for one representative public TCR and three exemplar private TCRs. As a collective molecular framework, these findings could inform the development of synergistic approaches to the prevention and/or treatment of bacterial diseases associated with the production of CDCs.

RESULTS

CD4$^+$ T cells recognize an immunodominant pneumolysin epitope

Ply is considered a potential candidate antigen for inclusion in a pneumococcal protein vaccine. We assessed the immunogenicity of a dPly by measuring antigen-specific proliferative responses in samples of human peripheral blood mononuclear cells (PBMCs). Using a tritium thymidine (^{3}HTdr) incorporation assay with a defined stimulation index (SI) cutoff of $\geq$2, we found that 81% of healthy donors (46/57) mounted proliferative responses against dPly (Figure 1A). We then used a 2D matrix layout incorporating 18mer peptides overlapping by 12 amino acids to screen the entire protein sequence of Ply for candidate CD4$^+$ T cell epitopes (Figure S1A). Three immunogenic peptide pools were identified among healthy donors (n = 10) (Figure S1B). Further screens using individual peptides from these pools revealed that S083-24 (Ply$_{427–444}$) elicited proliferative responses equivalent to those observed with dPly (Figure S1C). Of note, this immunodominant peptide (ECTGLAWEWWRTVYEKTD) spans the tryptophan (W)-rich region of Ply, incorporating the so-called "undecapeptide" sequence (ECTGLAWEWWR), which is functionally essential and highly conserved among CDCs.

In confirmatory experiments, we found that 72% of healthy donors (34/47) mounted proliferative responses against Ply$_{427–444}$ (Figure 1B), and using a flow cytometric dye dilution assay, we traced these responses to the CD4$^+$ T cell lineage (Figures 1C and 1D). We also found that responsive CD4$^+$ T cells produced IL-2 early after stimulation with Ply$_{427–444}$ and subsequently produced greater amounts of other cytokines, including interferon (IFN)-γ, IL-5, IL-13, IL-17A, and IL-22 (Figure 1E).

The prevalence of CD4$^+$ T cell responses against Ply$_{427–444}$ among healthy donors suggested antigen presentation in the context of multiple and/or very common HLA class II allomorphs. To map the relevant restriction element(s), we isolated three CD4$^+$ T cell clones that responded to Ply$_{427–444}$ *in vitro*, namely 198-93 from healthy donor 193, and 226-2E and 226-5F from healthy donor 226 (Table S1). Clonal proliferation in response to stimulation with dPly-loaded autologous B-lymphoblastoid cell lines (B-LCLs) was strongly inhibited by blocking antibodies directed against HLA-DP but not by blocking antibodies directed against HLA-DQ or HLA-DR (Figure 2A). The peptide-binding specificity of HLA-DP is thought to be dictated largely by expression of the polymorphic HLA-DP β-chain (DPB) allele, given that the HLA-DP α-chain (DPA) allele DPA1*01:03 is highly prevalent in the general population.[44,45] Using a panel of dPly-pulsed B-LCLs genotyped for HLA-DPB1, we found that clone 226-2E was most responsive to dPly-loaded HLA-DPB1*02:01, whereas clone 226-5F responded to dPly-loaded HLA-DPB1*02:01 and dPly-loaded HLA-DPB1*04:01, and clone 193-98 was most responsive to dPly-loaded HLA-DPB1*04:01 (Figure 2B). The allelic frequencies of HLA-DPB1*02:01 and HLA-DPB1*04:01 in the global population range up to 0.3500 and 0.5160, respectively,[46] giving rise to highly abundant phenotypic frequencies of up to 58%–77%.

Collectively, these data identify a highly immunogenic CD4$^+$ T cell epitope spanning the undecapeptide region of dPly, which elicits functionally diverse responses restricted by HLA-DPB1*02 and/or HLA-DPB1*04.

Pneumolysin undecapeptide-specific CD4$^+$ T cells are found after pneumococcal disease

To characterize the fine specificity of our CD4$^+$ T cell clones, we synthesized variants of the Ply$_{427–444}$ peptide, incorporating single alanine substitutions or various truncations, and performed a series of proliferation assays to test the impact of each modification on immunogenicity. These experiments revealed that the "core" epitopes were LAWEWWR for clone 226-2E, WEWWR for clone 226-5F, and GLAWEWWRTV for clone 193-98 (Figure S2A). Moreover, several alanine substitutions were not tolerated within these core epitopes (Figure S2B), indicating that the W-rich region was essential for CD4$^+$ T cell recognition and/or presentation by HLA-DPB1*02 and/or HLA-DPB1*04.

Sequence analysis further revealed that clones 226-5F and 193-98 expressed identical TCR α-chain (TRA) and TCR β-chain (TRB) gene segments (TRAV17/TRAJ32 and TRBV6-3/TRBJ2-7, respectively), with similar CDR3α (CATDKKGGATNKLIF and CATDARGGATNKLIF, respectively) and CDR3β loops (CASSQGGGEQYF and CASSDGGEQYF, respectively), whereas clone 226-2E expressed a distinct TCR, comprising TRAV4/CLVDSDGYALNF/TRAJ41 paired with TRBV7-2/CASSPPGVSGRLEQFF/TRBJ2-1. Of note, the alanine substitution at position (p)4 of the core epitope (LAWEWWR) abolished antigen recognition by clone 226-5F, which tolerated the corresponding substitutions at p3, p5, p6, and p7. In contrast, the peptide reactivity of clone 193-98 was highly sensitive to alanine substitution at p1, p3–p7, and p9, despite expression of a similar TCR (Figure S2B).

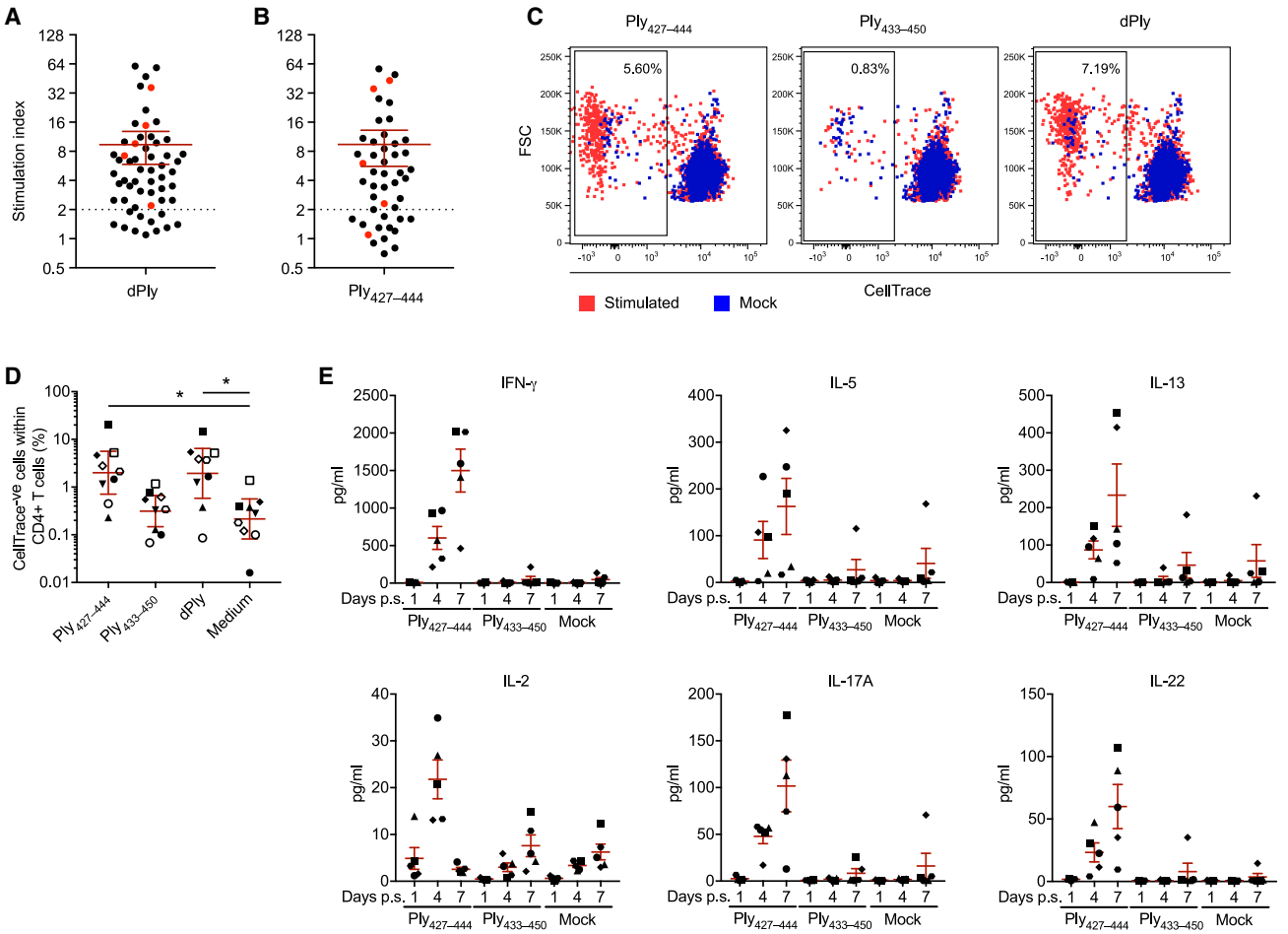

Figure 1. $Ply_{427–444}$ is an immunodominant epitope that induces $CD4^+$ T cell proliferation and cytokine production

(A) Proliferative responses were measured using a ^{3}HTdr incorporation assay after stimulation of healthy donor PBMCs (n = 57) with dPly. Each dot represents one donor and shows the mean of tests performed in triplicate. Red dots indicate donors selected for *ex vivo* HLA-DP*04/ECT tetramer-based index sorting and molecular analysis of expressed TCRs. Data are shown as mean ± SEM.

(B) Proliferative responses were measured using a ^{3}HTdr incorporation assay after stimulation of healthy donor PBMCs (n = 47) with the $Ply_{427–444}$ peptide. Each dot represents one donor and shows the mean of tests performed in triplicate. Red dots indicate donors selected for *ex vivo* HLA-DP*04/ECT tetramer-based index sorting and molecular analysis of expressed TCRs. Data are shown as mean ± SEM.

(C) Representative flow cytometry plots showing the dilution of CellTrace Violet among $CD4^+$ T cells after mock stimulation (blue) or stimulation (red) of healthy donor PBMCs with $Ply_{427–444}$ (left), $Ply_{433–450}$ (center), or dPly (right). Plots are gated on viable $CD3^+CD4^+CD8^-$ lymphocytes after aggregate exclusion. Percentage values indicate the frequencies of stimulated $CD4^+$ T cells with diluted CellTrace Violet.

(D) Pooled percentages from healthy donors (n = 9) derived as in (C). Each symbol represents one donor. Data are shown as mean ± SEM. *$p < 0.05$. Kruskal-Wallis test with Dunn's post hoc test.

(E) Cytokines were quantified in culture supernatants after mock stimulation or stimulation of healthy donor PBMCs (n = 5) with $Ply_{427–444}$ or $Ply_{433–450}$ for 1, 4, or 7 days (p.s., post-stimulation). Each symbol represents one donor and shows the mean of tests performed in triplicate. Data are shown as mean ± SEM.

See also Figure S1.

All three clones responded to $Ply_{427–439}$ (ECTGLAWEWWRTV), which encompasses the conserved undecapeptide sequence characteristic of the CDCs. We used this sequence (ECT) to generate HLA-DPB1*02:01/DPA1*01:03 and HLA-DPB1*04:01/DPA1*01:03 tetramers conjugated to phycoerythrin (PE). The respective HLA-DP*02/ECT and HLA-DP*04/ECT tetramers were validated against clones 226-2E, 226-5F, and 193-98, which bound HLA-DP*02/ECT, HLA-DP*02/ECT or HLA-DP*04/ECT, and HLA-DP*04/ECT, respectively (Figures 2C and 2D). We then used these tetramers in conjunction with the flow cytometric dye dilution assay to evaluate ECT-specific $CD4^+$ T cell responses in donors with a confirmed history of symptomatic IPDs (Table S1). For this purpose, PBMCs were collected longitudinally from a cohort of convalescent individuals (n = 6), all of whom expressed HLA-DPB1*04:01. Strong proliferative responses against dPly were maintained for up to 3 years from diagnosis in 5/6 donors, and substantial proportions of the responding $CD4^+$ T cell populations stained with the HLA-DP*04/ECT tetramer (Figure 2E). Using a direct *ex vivo* approach, we also detected HLA-DP*04/ECT-specific $CD4^+$ T cells among PBMCs from healthy genotype-matched donors (n = 5) with demonstrable responses against dPly (Figure 1A) and

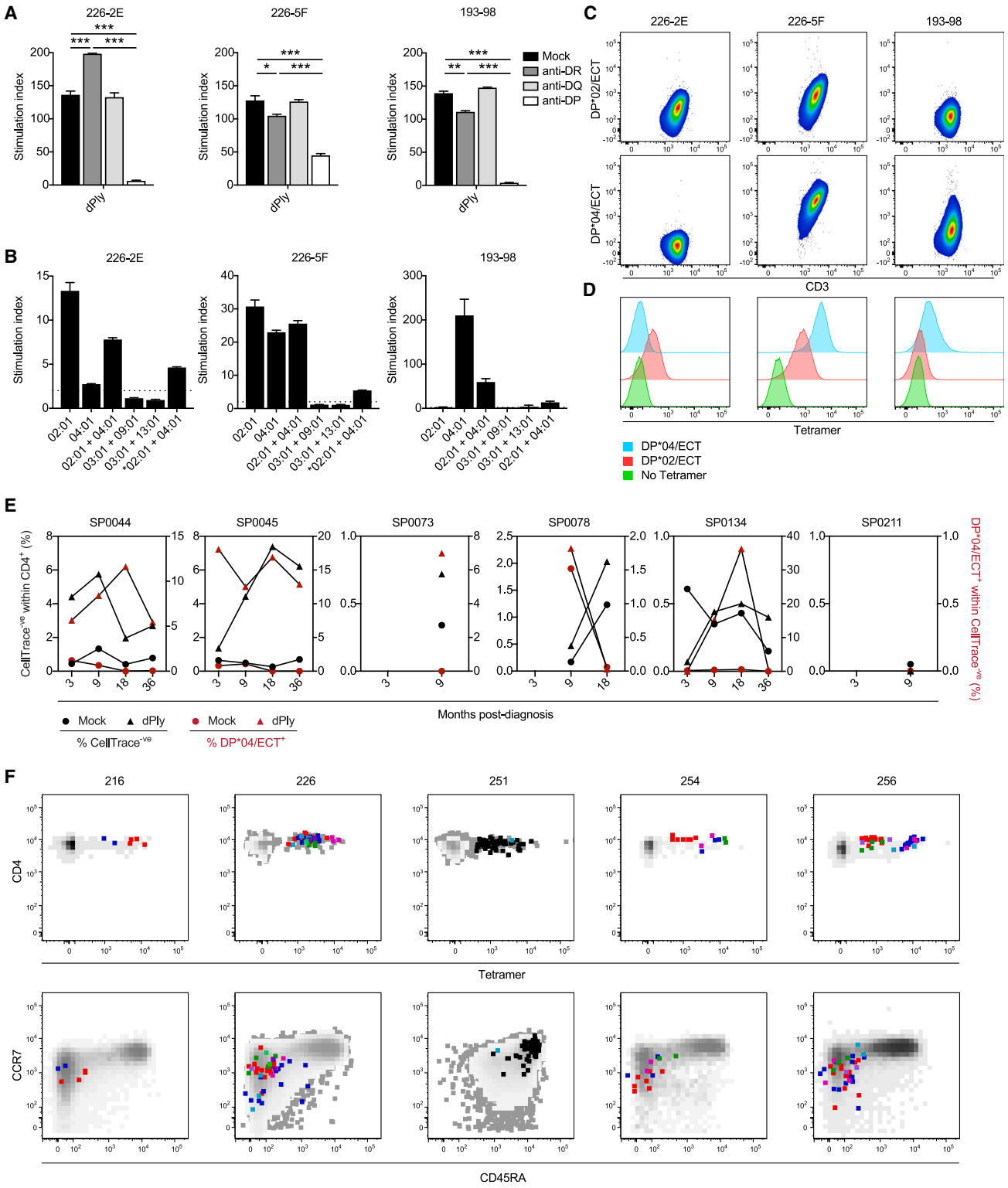

Figure 2. Memory CD4$^+$ T cell responses against Ply$_{427–444}$ are restricted by HLA-DPB1*02:01 and HLA-DPB1*04:01

(A and B) Proliferation of the CD4$^+$ T cell clones 226-2E, 226-5F, and 193-98 was measured using a ^{3}HTdr incorporation assay after stimulation with dPly-loaded autologous (A) or HLA-genotyped B-LCLs (B) in the absence (black bars) or presence of blocking antibodies directed against HLA-DR (dark gray bars), HLA-DQ (light gray bars), or HLA-DP (white bars). Asterisks indicate autologous B-LCLs in (B). Assays were performed in triplicate. Data are shown as mean ± SEM. *p < 0.05, **p < 0.01, and ***p < 0.001. One-way ANOVA with Tukey's post hoc test.

(legend continued on next page)

$Ply_{427–444}$ (Figure 1B), most of which exhibited a central memory ($CCR7^+CD45RA^-$) or an effector memory phenotype ($CCR7^-CD45RA^-$) (Figure 2F).

Collectively, these data show that Ply undecapeptide-specific $CD4^+$ T cells restricted by HLA-DP are present in convalescent donors after pneumococcal infection and form memory populations in healthy donors, likely reflecting prior exposure to *S. pneumoniae*.

Pneumolysin undecapeptide-specific $CD4^+$ T cells express genetically diverse TCRs

To establish a molecular basis for immune recognition of the Ply undecapeptide, we index-sorted HLA-DP*04/ECT tetramer-binding $CD4^+$ T cells from the healthy genotype-matched donors (n = 5) described above (Figure 2F) and sequenced the expressed TCRs (Table S1). We obtained a minimum of 13 and a maximum of 69 functional single-cell sequences per donor (Table S2). Analysis of the unique sequences revealed diverse gene use (Figures 3A–3D), a preference for CDR3α loops comprising 13 or 14 amino acids (Figure 3E), and no strong bias in favor of a particular CDR3β length (Figure 3F). Clonally expanded populations of memory $CD4^+$ T cells were nonetheless observed in 4/5 donors (Figures 2F and 3G). In contrast, only unique sequences were detected in donor 251, consistent with a naive-like phenotype ($CCR7^+CD45RA^+$) and a lack of expansion into memory (Figures 2F and 3G).

Among the paired single-cell sequences, we observed recurrent use of TRAV19/TRAJ22 in conjunction with TRBV7-3 and a segment from the TRBJ2 family (Table S2). We also identified a public TCR α-chain (TRA; TRAV19/CALSGSARQLTF/TRAJ22) in 3/5 donors (216, 226, and 251), which paired with TRBV7-3/CASSHREGETQYF/TRBJ2-5 in donor 216 (denoted hereafter as the B1 TCR) (Table S2). A near-identical TCR β-chain (TRB; TRBV7-3/CASSLREGDTQYF/TRBJ2-3) was present in 3/5 donors (251, 254, and 256) (Table S2). This sequence has previously been identified as public among bulk PBMCs.[47] For molecular comparison alongside the public B1 TCR, we selected two private sequences based on common gene use, namely TRAV4/CLVGDTGFQKLVF/TRAJ8 paired with TRBV20-1/CSARDPGGGGSSYEQYF/TRBJ2-7 from donor 254 (denoted hereafter as the B5 TCR) and TRAV8-3/CAVGANTGFQKLVF/TRAJ8 paired with TRBV20-1/CSARGDGYEQYF/TRBJ2-7 from donor 216 (denoted hereafter as the B8 TCR), and one private sequence based on uncommon gene use, namely TRAV17/CATDKKGGATNKLIF/TRAJ32 paired with TRBV6-3/CASSQGGGEQYF/TRBJ2-7 from donor 226 (denoted hereafter as the 5F TCR) (Table S2). This latter sequence was obtained from clone 226-5F.

Collectively, these data provide a genetic basis for $CD4^+$ T cell recognition of the Ply undecapeptide epitope, highlighting antigen engagement via a diverse array of TCRs.

Public and private TCRs bind strongly to HLA-DP4-$Ply_{427–441}$

To investigate the molecular basis of antigen recognition and clonal selection, we first used surface plasmon resonance (SPR) to measure the equilibrium affinity (K_D) and binding kinetics of the interactions between recombinant HLA-DP4/DP2-$Ply_{427–441}$ and soluble versions of each TCR (5F, B1, B5, and B8). The affinity values of each TCR for HLA-DP4-$Ply_{427–441}$ varied from ∼12 to ∼17 μM (Table 1; Figure S3), falling within the expected range for non-self/pathogen-derived epitope-specific TCRs.[48,49] The public B1 TCR and the private 5F TCR bound HLA-DP4-$Ply_{427–441}$ with similar kinetics, exhibiting faster on-rates (k_{on} = 48,400 $M^{-1}s^{-1}$ for B1 and 42,300 $M^{-1}s^{-1}$ for 5F) and off-rates (k_{off} = 0.7 s^{-1} for B1 and 5F) compared with the private TRBV20-1/TRBJ2-7$^+$ B5 and B8 TCRs (k_{on} = 20,800 $M^{-1}s^{-1}$ and k_{off} = 0.2 s^{-1} for B5; k_{on} = 12,700 $M^{-1}s^{-1}$ and k_{off} = 0.2 s^{-1} for B8) (Table 1; Figure S4). In line with the functional data, the 5F TCR, but not the B1, B5, or B8 TCRs, also bound HLA-DP2-$Ply_{427–441}$, albeit with low affinity (K_D ∼ 95 μM) and kinetics that were too fast to measure accurately (Figures S3 and S4).

$Ply_{427–441}$ forms a highly featured epitope in complex with HLA-DP4

To extend these findings, we solved the crystal structure of HLA-DP4-$Ply_{427–441}$ at a resolution of 3.0 Å (Table S3). The overall structure of this binary complex was similar to those of other reported HLA-DP-peptide complexes.[50–52] As anticipated, the $Ply_{427–441}$ epitope bound HLA-DP4 in a canonical conformation, with the side chains of p1-Leu, p4-Glu, p6-Trp, and p9-Val anchored in pockets P1, P4, P6, and P9, respectively. The peptide backbone bound HLA-DP4 via a network of fifteen hydrogen bonds (H-bonds) and three salt bridges (Figure S5A). The side chain of p4-Glu lay parallel to the base of the antigen-binding groove, forming H-bonds with Asn62α and Gln13β and salt bridges with Lys71β and Arg77β, thereby acting as an anchor residue. In the adjacent P6 pocket, the buried p6-Trp residue formed an H-bond with Asn62α and extensive van der Waals (vdW) contacts with Phe22α, Ala61α, Ile65α, Gly11β, Arg12β, Gln13β, Glu28β, Arg29β, and Tyr30β. The surface-exposed side chain of p7-Arg formed a salt bridge with Glu70β (Figure S5A). Accordingly, the solvent-exposed side chains of the $Ply_{427–441}$ residues p3-Trp, p5-Trp, p7-Arg, and p8-Thr were accessible for interactions with the TCR (Figures S5A and S5B).

(C and D) Staining of the $CD4^+$ T cell clones 226-2E, 226-5F, and 193-98 with HLA-DP*02/ECT and HLA-DP*04/ECT tetramers conjugated to PE. Plots are gated on viable $CD3^+CD4^+CD8^-$ lymphocytes after aggregate exclusion. Histogram overlays show the fluorescence-minus-one controls (D).

(E) PBMCs from convalescent individuals with a confirmed history of symptomatic IPDs (n = 6) were labeled with CellTrace Violet and then stained with the HLA-DP*04/ECT tetramer after mock stimulation (circles) or stimulation with dPly (triangles). All donors expressed HLA-DPB1*04:01. Graphs show the frequencies of $CD4^+$ T cells with diluted CellTrace Violet (black symbols) and the frequencies of $CD4^+$ T cells with diluted CellTrace Violet that were stained with the HLA-DP*04/ECT tetramer (red symbols) for each donor at the indicated time points after diagnosis.

(F) Flow cytometry plots showing direct *ex vivo* staining of healthy donor PBMCs with the HLA-DP*04/ECT tetramer (top) and the phenotype of HLA-DP*04/ECT tetramer-binding $CD4^+$ T cells (bottom). Plots are gated on viable $CD3^+CD8^-CD14^-CD19^-$ cells (top) or viable $tetramer^+CD3^+CD4^+CD8^-CD14^-CD19^-$ cells (bottom) after aggregate exclusion. Index-sorted cells are colored to match the TCR sequences displayed in Figure 3G. The turquoise dot in the overlays from donor 251 indicates the unexpanded public B1 TCR.

See also Figure S2 and Table S1.

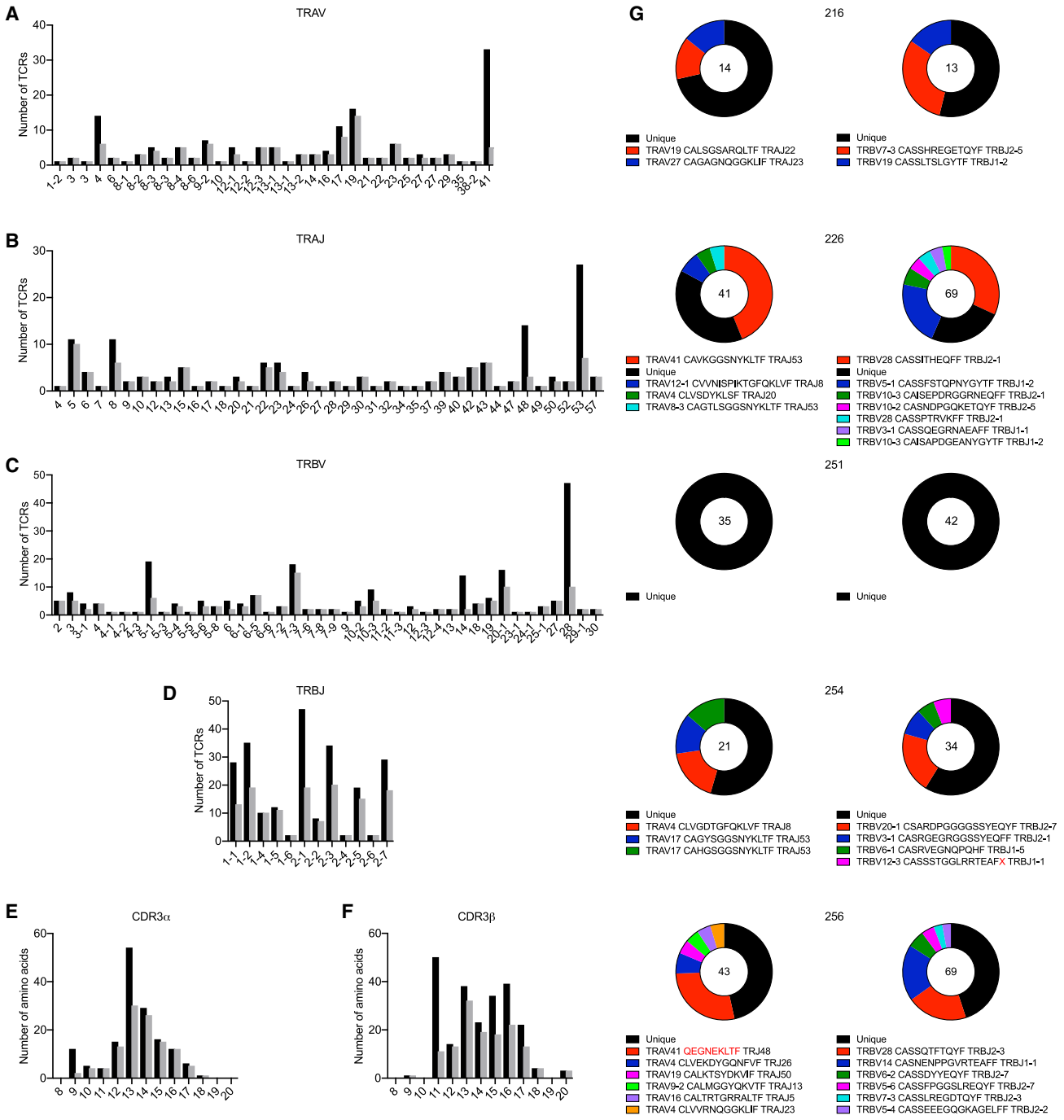

Figure 3. $Ply_{427–439}$ is targeted by architecturally diverse TCRs

HLA-DP*04/ECT tetramer-binding $CD4^+$ T cells from healthy donors (n = 5) were index-sorted directly *ex vivo*, and a multiplex approach was used to sequence the expressed TCRs.

(A–D) Use of TRAV (A), TRAJ (B), TRBV (C), and TRBJ gene segments (D). Data were pooled to include all obtained (black bars) or unique sequences (gray bars).

(E and F) CDR3α (E) and CDR3β lengths (F). Data were pooled to include all obtained (black bars) or unique sequences (gray bars).

(G) Summary of individual donor repertoires detailing clonally expanded TCRs. Red font denotes poor read quality. The number of sequences obtained per repertoire is shown in each circle. Recurrent sequences are colored to match the index displays in Figure 2F.

See also Table S2.

Table 1. Affinity and kinetics measurements

TCR-HLA-DP-Ply	K_{Deq}	B_{max}	k_{on}	k_{off}	K_{Dcal}	$t_{1/2}$
5F-HLA-DP4-Ply	15.54 ± 1.22	723.7	42.3 ± 6.9	0.689 ± 0.096	16.33 ± 0.56	1.01
B1-HLA-DP4-Ply	14.93 ± 0.78	747.0	48.4 ± 6.0	0.722 ± 0.065	14.96 ± 0.62	0.96
B5-HLA-DP4-Ply	11.48 ± 0.68	794.5	20.8 ± 1.4	0.244 ± 0.013	11.76 ± 0.39	2.84
B8-HLA-DP4-Ply	17.34 ± 0.65	830.1	12.7 ± 1.2	0.222 ± 0.018	17.52 ± 0.36	3.12
5F-HLA-DP2-Ply	95.33 ± 4.29	691.0	ND	ND	ND	ND

K_{Deq} and K_{Dcal} are in μM; k_{on} is in M^{-1} s^{-1} × 10^3; k_{off} is in s^{-1}; $t_{1/2}$ is in s. ND, not determined. Data are shown as the mean of two independent experiments performed in duplicate ± SD.

Exemplar private TCRs engage common regions of HLA-DP4-Ply$_{427–441}$

To understand immune recognition of this highly featured epitope, we first solved the crystal structures of the private TRBV6-3/TRBJ2-7$^+$ 5F (resolution = 2.8 Å) and TRBV20-1/TRBJ2-7$^+$ B5 TCRs (resolution = 3.1 Å) in complex with HLA-DP4-Ply$_{427–441}$ (Table S3). The α- and β-chains of each TCR were positioned above the β- and α-chains of HLA-DP4, respectively, adopting a canonical docking polarity (Figures 4A and 4B).[49]

The 5F TCR docked at an angle of ∼66° across the antigen-binding cleft of HLA-DP4, with an overall buried surface area (BSA) of 1,950 Å^2. Relative contributions to the overall BSA at the 5F TCR-HLA-DP4-Ply$_{427–441}$ interface were 18%, 17%, 16%, and 9% for CDR2β, CDR1β, CDR3β, and the β-framework (FWβ) region, respectively, and 28%, 7%, and 5% for CDR3α, CDR2α, and CDR1α, respectively (Figure 4A). The 5F TCR interacted with the bound peptide and both chains of HLA-DP4 (Figures 5A and 5B; Table S4). Three germline-encoded residues, namely CDR1α Asn37α and CDR2α Arg57α and Asn59α, formed vdW contacts with the HLA-DP4 β-chain residues Arg77β, Ala73β, and Asp76β, respectively. This combination of TRA residues is unique to TRAV13-1, which was observed in the antigen-specific repertoire dataset (Figure 3A), and TRAV17, employed by the 5F TCR. Moreover, CDR1β Asn28β, Glu37β, and Tyr38β, CDR2β Val57β, Gly58β, Glu63β, and Thr65β, and the FWβ residues ^{66}Thr-Ala^{67}, which in combination are unique to TRBV6-2 and TRBV6-3, were involved in interactions with the bound peptide and both chains of HLA-DP4 (Figures 5A and 5B; Table S4). Specifically, the CDR1β loop interacted with the β-chain of HLA-DP4, where Asn28β bound Tyr60β and Glu37β bound Ile67β. The CDR1β loop also interacted with the solvent-exposed side chains of the bound peptide at p5-Trp, p7-Arg, and p8-Thr, where Glu37β formed polar contacts with p7-Arg and p8-Thr, and Tyr38β formed vdW contacts with p5-Trp and an H-bond with p7-Arg. In addition, the CDR2β loop residue Val57β bound p5-Trp and the HLA-DP4 α-chain residues Ala61α and Ile65α, whereas Glu63β was H-bonded to Asn68α, Thr65β contacted Ala61α and Ala64α, and the neighboring FWβ ^{66}Thr-Ala^{67} residues interacted with Gln57α (Figures 5A and 5B; Table S4).

The interface with the bound peptide was formed by the CDR3α, CDR1β, CDR2β, and CDR3β loops of the 5F TCR. The CDR3α motif ^{110}Gly-Gly-Ala-Thr-Asn^{114}, which is exclusive to TRAJ32, interacted with the bound peptide and HLA-DP4 (Figures 5A and 5B; Table S4). Here, the CDR3α residues Gly110α and Gly111α contacted p3-Trp and the HLA-DP4 α-chain residue Glu55α, Ala112α interacted with p3-Trp and p5-Trp, and Asn114α formed an H-bond with p5-Trp. In addition, the CDR3α residue Thr113α interacted with p3-Trp, p5-Trp, and the HLA-DP β-chain residue Arg77β. The CDR3β loop interacted minimally with the bound peptide via an H-bond between the non-templated residue Gln108β and p7-Arg. The non-germline-encoded CDR3β residue Gly113β formed a H-bond with Glu70β, and the side chains of Gln108β and the TRBJ2-7 segment residue Tyr117β interacted with Asp66β (Figures 5A and 5B; Table S4).

The B5 TCR docked at an angle of ∼86° across the antigen-binding cleft of HLA-DP4, with an overall BSA of 2,310 Å^2. Relative contributions to the overall BSA at the B5 TCR-HLA-DP4-Ply$_{427–441}$ interface were 29%, 7%, and 11% for CDR3β, CDR2β, and CDR1β, respectively, and 20%, 18%, and 9% for CDR1α, CDR3α, and CDR2α, respectively (Figure 4B). Akin to the 5F TCR, the B5 TCR interacted with the bound peptide and both chains of HLA-DP4 (Figures 5C and 5D; Table S5). The structural determinants of TRAV4 bias were attributable to a unique set of germline-encoded residues, namely CDR1α Thr30α, Asn36α, and Tyr38α, CDR2α Tyr57α and Lys58α, and FWα Gln55α. Here, Thr30α contacted the HLA-DP4 β-chain residues Asp76β, Arg77β, and His81β, whereas Asn36α formed vdW contacts with p2-Ala and His81β, and Tyr38α interacted with Glu70β. The CDR2α residues Tyr57α and Lys58α were both H-bonded to Asp76β, whereas Thr64α interacted with Glu69β, and the FWα residue Gln55α formed an H-bond with Glu70β (Figures 5C and 5D; Table S5). TRBV20-1 use was similarly attributable to unique germline-encoded residues, namely CDR1β Gln29β and Thr37β and CDR2β Asn57β and Glu58β, which interacted exclusively with the α-chain of HLA-DP. Here, Gln29β and Thr37β were H-bonded to Asn68α and Gln57α, respectively, and also contacted Ala64α and Ala61α, respectively, whereas Asn57β formed vdW contacts with Gln57α, and Glu58β was H-bonded to Lys39α (Figure 5D).

The ternary structure of the B5 TCR in complex with HLA-DP4-Ply$_{427–441}$ also revealed a requirement for the CDR3α motif ^{111}Thr-Gly-Phe-Gln^{114} (Figures 5C and 5D; Table S5), which is unique to TRAJ8. In particular, Thr111α interacted with p3-Trp, p5-Trp, and the HLA-DP4 β-chain residue Arg77β, whereas Gly112α and Gln114α mediated vdW contacts with the HLA-DP4 α-chain residue Glu55α, and Phe113α formed an H-bond and vdW contacts with the HLA-DP4 α-chain residues Glu55α and Gln57α, respectively. Moreover, Asp108α and Gly112α contacted p3-Trp, and Phe113α contacted p5-Trp. Of note, the CDR3β loop of the B5 TCR incorporated a string of four non-germline-encoded glycine

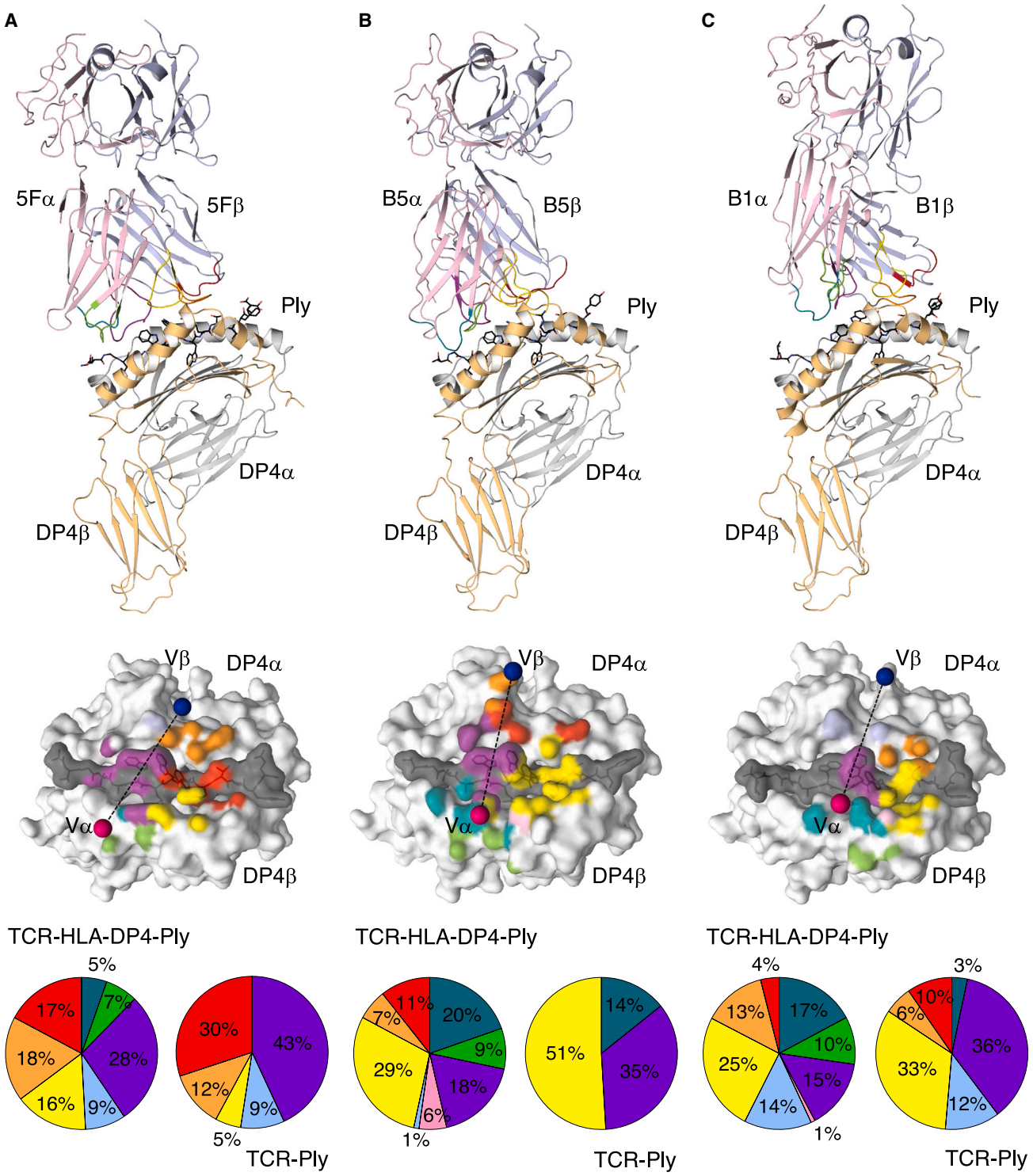

Figure 4. Structural overview of public and private TCRs in complex with HLA-DP4-Ply$_{427-441}$

Top: the α- and β-chains of the 5F (A), B5 (B), and B1 TCRs (C) are shown in light pink and light blue, respectively, Ply is shown in black, and the α- and β-chains of HLA-DP4 are shown in light gray and light orange, respectively. The corresponding CDR1α, CDR2α, CDR3α, CDR1β, CDR2β, and CDR3β loops are shown in teal, green, purple, red, orange, and yellow, respectively. Middle: footprints of the 5F (A), B5 (B), and B1 TCRs (C) on the surface of HLA-DP4-Ply. Each docking angle is shown as a black dashed line connecting the center of mass of Vα (dark pink sphere) with the center of mass of Vβ (dark blue sphere). HLA-DP4 is colored light gray, and Ply is colored dark gray. TCR segment colors as in (A). Bottom: pie charts depicting the relative contribution of each segment of the 5F (A), B5 (B), and B1 TCRs (C) to the buried surface area (BSA) directed against HLA-DP4-Ply (left) or Ply alone (right). TCR segment colors as in (A).

See also Figures S3–S5 and Tables S3–S6.

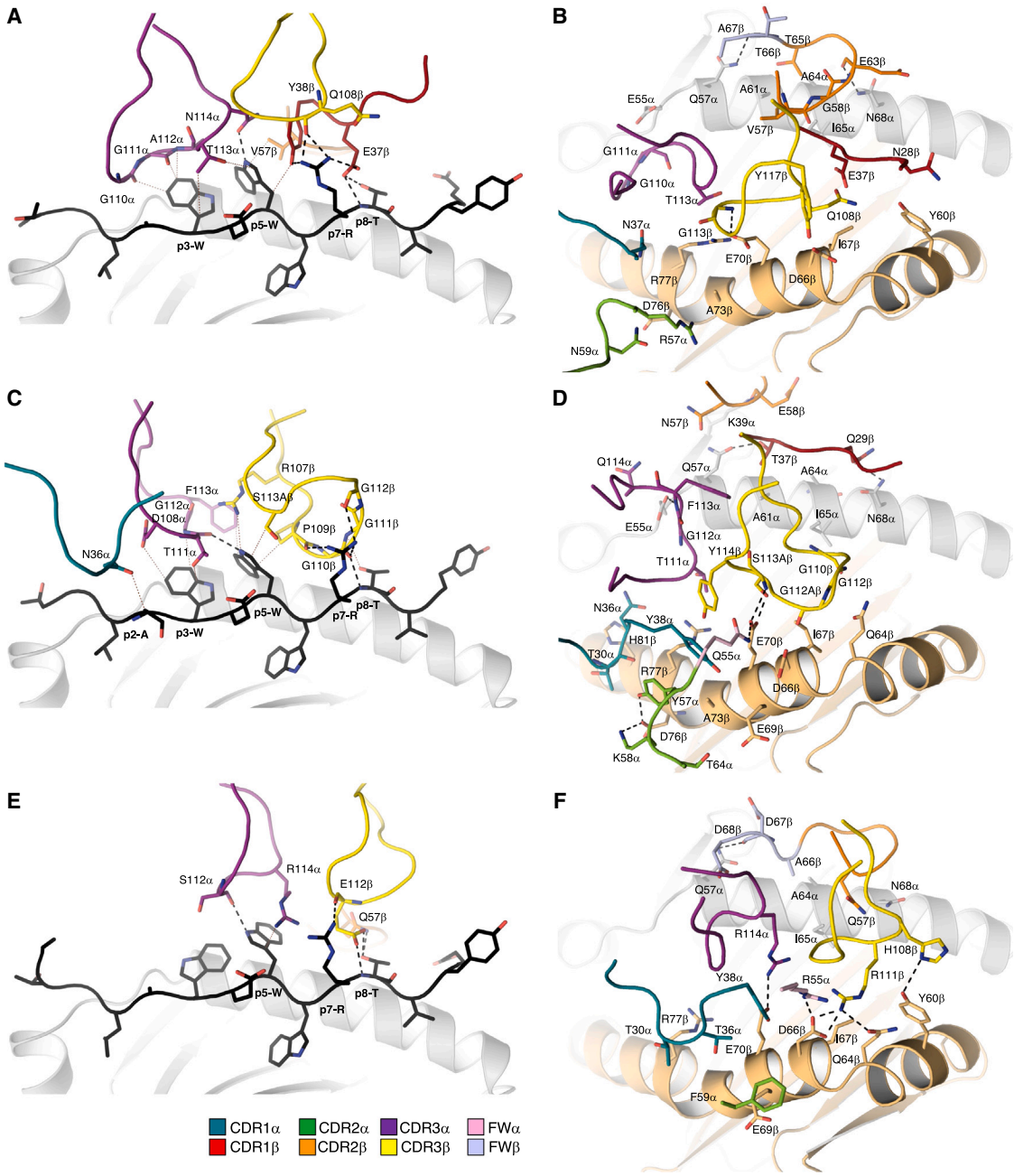

Figure 5. Interface comparison of public and private TCRs in complex with HLA-DP4-Ply$_{427–441}$

(A, C, and E) Interactions between Ply and the 5F (A), B5 (C), and B1 TCRs (E). Ply is shown in black. The corresponding CDR1α, CDR2α, CDR3α, CDR1β, CDR2β, and CDR3β loops are shown in teal, green, purple, red, orange, and yellow, respectively, and the corresponding framework (FW) residues of the α- and β-chains are shown in light pink and light blue, respectively.

(B, D, and F) Interactions between HLA-DP4 and the 5F (B), B5 (D), and B1 TCRs (F). The α- and β-chains of HLA-DP4 are shown in light gray and light orange, respectively. TCR segment colors as in (A, C, and E). Interacting residues are shown as sticks, hydrogen bonds are shown as black dashes, and van der Waals (vdW) contacts are shown as brown dashed lines.

See also Figures S3–S5 and Tables S3–S6.

residues, which formed a series of H-bonds with the side-chain polar group of p7-Arg and vdW interactions with the HLA-DP4 α-chain residue Ile65α and the HLA-DP4 β-chain residues Gln64β, Asp66β, and Ile67β. The CDR3β residues Arg107β and Pro109β interacted with p5-Trp, and Pro109β was also H-bonded to p7-Arg. The TRBJ2-7 segment contributed Ser113β, which formed vdW contacts with p5-Trp and H-bonds with the HLA-DP4 β-chain residue Glu70β, and Tyr114β, which interacted with the HLA-DP4 β-chain residues Glu70β and Arg77β (Figures 5C and 5D; Table S5).

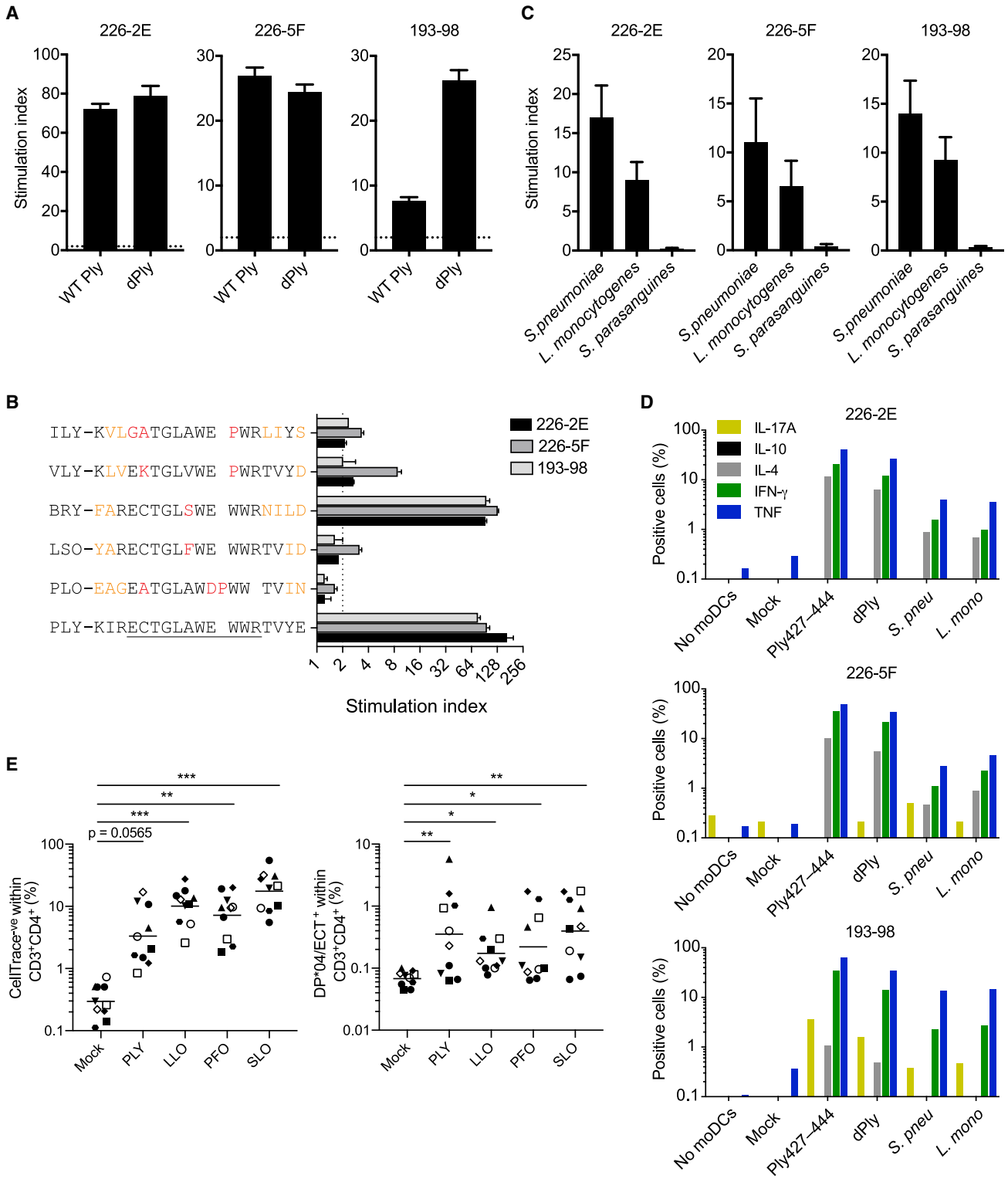

Figure 6. Cross-recognition profiles of undecapeptide-specific CD4⁺ T cell clones

(A) Proliferation of the CD4⁺ T cell clones 226-2E, 226-5F, and 193-98 was measured using a ^{3}HTdr incorporation assay after stimulation with heat-inactivated wild-type (WT) Ply-loaded or dPly-loaded autologous B-LCLs. Assays were performed in triplicate. Data are shown as mean ± SEM.

(B) Proliferation of the CD4⁺ T cell clones 226-2E, 226-5F, and 193-98 was measured using a ^{3}HTdr incorporation assay after stimulation with peptide-loaded autologous B-LCLs. Red font indicates amino acid residues in the undecapeptide region that differ from Ply, and orange font indicates amino acid residues in the epitope-flanking region that differ from Ply. Assays were performed in duplicate. Data are shown as mean ± SEM.

(legend continued on next page)

Collectively, these data show that private TCRs can engage all solvent-exposed residues of the bound peptide, namely p3-Trp, p5-Trp, p7-Arg, and p8-Thr, as well as common HLA-DP4 α-chain (Glu55α, Gln57α, Ile65α, Ala61α, Ala64α, and Asn68α) and β-chain residues (Asp66β, Ile67β, Glu70β, and Arg77β). In addition, structural requirements for unique germline-encoded residues explain the selection of particular TRAV/TRBV gene segments, which constitute the CDR1/2 loops, as well as TRAJ8/TRAJ32 via the positionally equivalent residues Thr113α (5F) and Thr111α (B5) and TRBJ2-7 via residues Tyr117β (5F) and Ser113β/Tyr114β (B5).

A public TCR uses recurrent gene segments to engage HLA-DP4-Ply$_{427–441}$

To extend these findings, we solved the crystal structure of the public TRAV19/TRBV7-3$^+$ B1 TCR in complex with HLA-DP4-Ply$_{427–441}$ at a resolution of 3.4 Å (Table S3). The B1 TCR docked at an angle of ∼78° across the antigen-binding cleft of HLA-DP4, with an overall BSA of 1,800 Å^2. Relative contributions to the overall BSA at the B1 TCR-HLA-DP4-Ply$_{427–441}$ interface were 25%, 13%, 4%, and 14% for CDR3β, CDR2β, CDR1β, and FWβ, respectively, and 17%, 15%, 10%, and 1% for CDR1α, CDR3α, CDR2α, and FWα, respectively (Figure 4C). The overall structure of HLA-DP4-Ply$_{427–441}$ was largely unaltered in the liganded state, with a root mean square deviation of ∼0.3 Å for HLA-DP4 α-chain residues across 1–180 atoms for all protomers compared with the binary structure (Figures S5A and S5B).

Akin to the private 5F and B5 TCRs, the public B1 TCR interacted with the bound peptide and both chains of HLA-DP4 (Figures 5E and 5F; Table S6). The CDR1α and CDR2α loops contacted the β-chain of HLA-DP4, the CDR3α and CDR3β loops contacted the bound peptide, and the CDR2β loop contacted the α-chain of HLA-DP4. A combination of residues unique to TRAV19, namely CDR1α Thr30α, Thr36α, and Tyr38α, CDR2α Phe59α, and FWα Arg55α, mediated contacts with the β-chain of HLA-DP4. Two of these key residues, namely Thr30α and Tyr38α, occur otherwise only in TRAV4, employed by the B5 TCR. The CDR1α residues Thr30α and Thr36α bound Arg77β and Glu70β, respectively, whereas Tyr38α bound Asp66β and contacted Glu70β within H-bond distance. In addition, the side chain of the CDR2α residue Phe59α bound Glu69β, and the FWα residue Arg55α contacted Asp66β within H-bond distance. Use of the TRBV7-3 segment was driven by a unique combination of residues, namely Gln57β and the FWβ motif ^{66}Ala-Asp-Asp^{68}, which contacted the α-chain of HLA-DP4. Of note, the CDR2β residue Gln57β formed vdW contacts with Ile65α and Asn68α and also contacted p8-Thr within H-bond distance, whereas the FWβ motif residues bound Gln57α and Ala64α (Figures 5E and 5F; Table S6).

Specific interactions between the B1 TCR and the bound peptide were mediated by the CDR3α, CDR2β, and CDR3β loops via the TRAJ22-exclusive CDR3α residues Ser112α and Arg114α, the CDR2β residue Gln57β, and the non-templated CDR3β residues Arg111β and Glu112β. The CDR3α motif ^{112}Ser-Ala-Arg^{114} motif formed a bridge between p5-Trp and Glu70β, whereas the CDR3β motif ^{111}Arg-Glu^{112} contacted p7-Arg and p8-Thr. In addition, Arg111β contacted the HLA-DP4 β-chain residues Gln64β, Asp66β, and Ile67β (Figures 5E and 5F; Table S6). The non-templated CDR3β residue His108β bound the HLA-DP4 β-chain residue Tyr60β, which was also contacted by the private 5F TCR CDR1β residue Asn28β (Figure 5F).

The public B1 TCR docked closer to the peptide C terminus of HLA-DP4-Ply$_{427–441}$ than the private 5F and B5 TCRs, limiting contacts with the bound peptide to the solvent-exposed residues p5-Trp, p7-Arg, and p8-Thr. As a consequence, the CDR3α loop interacted with HLA-DP4 β-chain residue Glu70β, which was otherwise contacted by the CDR3β loops of the private 5F and B5 TCRs. The public B1 TCR nonetheless interacted with the HLA-DP4 residues Gln57α, Ala64α, Ile65α, Asn68α, Asp66β, Ile67β, Glu70β, and Arg77β, all of which were also contacted by the private 5F and B5 TCRs.

Collectively, these observations provide a rationale for the recurrent selection of particular gene segments in the HLA-DP4-Ply$_{427–441}$ epitope-specific repertoire dataset and identify key structural differences and similarities between the public B1 TCR and the private 5F and B5 TCRs.

Pneumolysin-specific CD4$^+$ T cells cross-recognize other bacterial CDCs

To explore the broader implications of our findings, we tested the ability of the CD4$^+$ T cell clones 198-93, 226-2E, and 226-5F to cross-recognize the undecapeptide region of wild-type Ply, which lacks the detoxifying mutation Cys428Gly. All three clones were functionally reactive against synthetic peptides containing the wild-type Cys428 residue (Figure S2A) and naturally processed forms of heat-inactivated Ply, although clone 193-98 exhibited a marked preference for dPly (Figure 6A).

At least 28 bacterial species from divergent phyla are known to produce CDCs,[21,53] of which 22, including Ply and other prominent examples, such as listeriolysin O (LLO) from *Listeria monocytogenes*, perfringolysin O (PFO) from *Clostridium perfringens*, and streptolysin O (SLO) from *Streptococcus pyogenes*, have an identical undecapeptide region. In contrast, the undecapeptide region varies across the other known CDCs, namely pyolysin (PLO) from *Actinomyces pyogenes* (Cys428Ala, Glu434Asp, Glu434/Trp435insPro, Arg437del), intermedilysin (ILY) from *Streptococcus intermedius* (Glu427Gly, Cys428Ala, Trp435Pro), vaginolysin (VLY) from *Gardenella vaginalis* and lectinolysin (LLY)

(C) Proliferation of the CD4$^+$ T cell clones 226-2E, 226-5F, and 193-98 was measured using a ^{3}HTdr incorporation assay after stimulation with heat-inactivated *S. pneumoniae*-loaded, *L. monocytogenes*-loaded, or *S. parasanguines*-loaded autologous moDCs. Assays were performed in quadruplicate. Data are shown as mean ± SEM.

(D) Intracellular cytokine production by the CD4$^+$ T cell clones 226-2E, 226-5F, and 193-98 was measured via flow cytometry in the absence of moDCs or after stimulation with mock-loaded, Ply$_{427–444}$-loaded, dPly-loaded, heat-inactivated *S. pneumoniae*-loaded, or heat-inactivated *L. monocytogenes*-loaded autologous moDCs.

(E) PBMCs from healthy donors (n = 10) were labeled with CellTrace Violet and then stained with the HLA-DP*04/ECT tetramer after mock stimulation (circles) or stimulation with Ply, LLO, PFO, or SLO. All donors expressed HLA-DPB1*04:01. Graphs show the frequencies of CD4$^+$ T cells with diluted CellTrace Violet (left) and the frequencies of CD4$^+$ T cells that stained with the HLA-DP*04/ECT tetramer (right). Each symbol represents one donor. Horizontal bars indicate mean values. *p < 0.05, **p < 0.01, ***p < 0.001. Kruskal-Wallis test with Dunn's post hoc test comparing each condition versus mock.

from *Streptococcus mitis* (Cys428Lys, Ala432Val, Trp435Pro), butyriculysin (BRY) from *Clostridium butyricum* (Ala432Ser), and seeligeriolysin (LSO) from *Listeria seeligeri* (Ala432Phe).[21,53] Using autologous B-LCLs to present synthetic peptides mimicking these non-conserved epitopes with natural flanking residues, we found that all three clones responded strongly to the BRY variant and moderately to the ILY and VLY variants, whereas only clone 226-5F cross-recognized the LSO variant, and none of the clones cross-recognized the PLO variant (Figure 6B).

In further experiments designed to assess the efficacy of natural antigen processing and presentation, we found that all three clones proliferated strongly in response to autologous monocyte-derived DCs (moDCs) loaded with heat-inactivated whole-cell preparations of *S. pneumoniae* or *L. monocytogenes* but not with a heat-inactivated whole-cell preparation of *S. parasanguines*, which lacks a CDC (Figure 6C). Moreover, clones 226-2E and 226-5F produced tumor necrosis factor (TNF), IFN-γ, and IL-4, whereas clone 193-98 produced TNF, IFN-γ, IL-17A, and low amounts of IL-4, in response to moDCs loaded with the $Ply_{427–444}$ peptide, dPly, heat-inactivated *S. pneumoniae*, or heat-inactivated *L. monocytogenes*, indicating consistent response patterns across each condition (Figure 6D). To link these findings with epitope specificity, we stimulated PBMCs from healthy donors (n = 10) with heat-inactivated Ply, LLO, PFO, or SLO. After 7 days, strong proliferative responses were observed among $CD4^+$ T cells exposed to each of these CDCs, and importantly, HLA-DP*04/ECT tetramer-binding $CD4^+$ T cells were clearly identifiable in 6/10, 4/10, 4/10, and 7/10 cases following stimulation with Ply, LLO, PFO, or SLO, respectively (Figure 6E).

Collectively, these data show that Ply-specific $CD4^+$ T cells focused on a single immunodominant epitope restricted by HLA-DP efficiently cross-recognize bacterial species expressing undecapeptide-identical CDCs and, to some extent, bacterial species expressing variant CDCs.

DISCUSSION

$CD8^+$ T cell-mediated antigen recognition has been studied extensively in the context of viral infections, and the ternary structures of various public αβ TCRs have been elucidated in complex with epitopes derived from influenza virus,[54,55] Epstein-Barr virus (EBV),[56–58] human cytomegalovirus (HCMV),[59] and human immunodeficiency virus type 1 (HIV-1).[60] These studies have provided key insights into the molecular rules that govern the biased selection of αβ TCRs, which occurs to a variable extent across all $CD8^+$ T cell repertoires with defined antigen specificity.[61,62] In contrast, relatively little is known about $CD4^+$ T cell-mediated antigen recognition in the context of bacterial infections, and it has remained unclear to what extent such principles guide the selection of HLA-class-II-restricted αβ TCRs.

In this study, we identified public and private $CD4^+$ T cell clonotypes specific for the highly immunodominant pneumococcal epitope $Ply_{427–444}$, which is presented by the globally abundant allomorphs HLA-DPB1*02:01 and HLA-DPB1*04:01.[63] Among healthy HLA-$DP4^+$ adults, public and near-public αβ TCRs commonly incorporated the TRAV19/TRAJ22 and TRBV7-3/TRBJ2-3/5/7 gene segments, whereas private αβ TCRs commonly incorporated the TRBV20-1 and/or TRBJ2-7 gene segments, all of which contributed non-redundant contact residues that engaged the cognate antigen in structural analyses of one representative public TCR (B1) and three exemplar private TCRs (5F, B5, and B8). It was also notable that the public CDR3β motif (CASSXREGXTQYF) matched recurrent sequences detected in previous studies of bulk PBMCs.[47,64,65]

Each of the four recombinant TCRs studied here bound HLA-DP4-Ply with a similar equilibrium affinity. In addition, the 5F TCR bound HLA-DP2-Ply, consistent with the functional data obtained using clone 226-5F. Cross-allomorph recognition has been examined previously in the context of TCRs specific for immunodominant epitopes derived from the p24 capsid protein of HIV-1.[66,67] In these instances, cross-recognition was attributable to a peptide-centric mode of engagement, alongside key contacts with the HLA-DR α-chain.[67] We used proliferation assays to assess the extent to which the Ply-specific $CD4^+$ T cell clones 226-2E, 226-5F, and 193-98 cross-reacted against synthetic undecapeptide variants representing naturally occurring sequences and heterologous bacterial pathogens from divergent phyla expressing whole CDCs. As expected, all three clones responded equally well to *L. monocytogenes* and *S. pneumoniae*, which express undecapeptide-identical CDCs. In a similar vein, heat-inactivated preparations of other undecapeptide-identical CDCs, namely LLO, PFO, and SLO, rapidly mobilized HLA-DP*04/ECT tetramer-binding $CD4^+$ T cell populations directly *ex vivo*, indicating cross-species immune convergence on a single epitope specificity. The private 226-5F clone proliferated only when the core undecapeptide epitope p3-Trp-Glu-Trp-Trp-Arg-p7 was intact, as in BRY (ECTGLSWEWWR) and LSO (ECTGLFWEWWR), or nearly intact, as in ILY (GATGLAWEPWR) and VLY (EKTGLVWEPWR). Moreover, structural analysis revealed that the public B1 TCR and the private 5F and B5 TCRs were focused on residues p3 and/or p5, p7, and p8, whereas the buried p4 residue was anchored to HLA-DP4. The conserved p3-WEWWR-p7 motif was therefore critical for immune cross-recognition of bacterial CDCs.

The undecapeptide sequence plays a critical role in the functionality of CDCs, facilitating membrane insertion, refolding, oligomerization, and pore formation, which ultimately trigger cell death.[22–28] It is tempting to propose a link between these roles and the pervasive antigenicity of this particular region, which elicited response rates in our cohort that exceeded 70%. One possible explanation here is that cells permeabilized by bacterial toxins can employ membrane-resealing mechanisms to evade cytotoxicity, such as the internalization of transmembrane pores into vacuolar vesicles that traffic to lysosomes for degradation, as demonstrated previously for SLO.[68] Such a mechanism could funnel degraded CDCs into the antigen processing pathway for presentation via MHC class II, enabled by a highly favorable motif for binding to the prevalent allomorphs HLA-DPB1*02:01 and HLA-DPB1*04:01.[69]

$CD4^+$ T cell-mediated immunity against Ply has been implicated in immune surveillance and pathogen elimination.[43,70] In this study, we found that the HLA-DP-restricted undecapeptide specificity was a prominent component of the Ply-directed $CD4^+$ T cell response, enabling widespread immunity against phylogenetically diverse bacterial pathogens linked by the expression of CDCs as a consequence of allomorph prevalence, antigen conservation, and epitope recognition via architecturally diverse public and private TCRs. A single and near-universal specificity

that "(almost) fits all" has not been documented previously in the context of the vast heterogeneity that characterizes adaptive $CD4^+$ T cell immunity. It should be noted that we did not address the biological relevance of undecapeptide-specific $CD4^+$ T cells beyond a simple analysis of the corresponding cytokine profiles in response to antigen stimulation, which suggested beneficial functions but did not exclude the possibility of a detrimental role, such as might be imparted by decoy activity or immune regulation. Other questions were also unresolved by the present work, including the possibility of coevolution between the HLA-DPB1 locus and bacterial pathobionts expressing CDCs, which could potentially explain the widespread prevalence of HLA-DPB1*02:01 and HLA-DPB1*04:01. Although further studies are warranted to clarify these issues and define the tissue distribution and protective capabilities of undecapeptide-specific $CD4^+$ T cells, our collective functional and molecular data have nonetheless provided key mechanistic insights that could accelerate the development of effective immunotherapeutics and/or vaccines to combat a broad range of bacterial diseases, including IPDs.

Limitations of the study

It is important to emphasize that our study provides no evidence that $CD4^+$ T cell-mediated recognition of $Ply_{427–444}$ confers immune protection against IPDs. Animal models and/or human challenge studies will likely be required to resolve this issue. Moreover, our study was confined to an examination of $CD4^+$ T cell responses in the vascular circulation, which might not reflect the immune landscape in tissues susceptible to colonization. Additional work profiling mucosal immunity at these sites across a range of clinical outcomes could provide more detailed insights into the factors that prevent invasion and clarify the role of tissue-localized $CD4^+$ T cells that recognize $Ply_{427–444}$ and related epitopes as sentinels of defense against bacterial diseases associated with the production of CDCs.

STAR★METHODS

Detailed methods are provided in the online version of this paper and include the following:

SUPPLEMENTAL INFORMATION

Supplemental information can be found online at https://doi.org/10.1016/j.immuni.2023.03.020.

ACKNOWLEDGMENTS

We thank Josien Lanfermeijer (RIVM/IIV) for technical support, Frans Reubsaet (RIVM/IDS) for providing clinical bacterial isolates, Marien de Jonge (Radboud UMC) for providing $TIGR4_{\Delta CPS}$, Sanofi Pasteur for providing Ply and dPly, the NIH Tetramer Core Facility for providing the HLA-DP*02/ECT and HLA-DP*04/ECT tetramers, and staff at the Monash Macromolecular Crystallization Facility and the Australian Synchrotron (beamlines MX1 and MX2) for assistance with crystallization and data collection, respectively. This study was funded by the Dutch Ministry of Health, Welfare and Sport (VWS). D.A.P. was supported by a Wellcome Trust Senior Investigator Award (100326/Z/12/Z). J.R. was supported by an NHMRC Investigator Award (L3).

AUTHOR CONTRIBUTIONS

L.C., M.D.B.v.d.G., and K.L. performed experiments, analyzed data, and wrote the paper; C.F., M.C.M.P., K.L.M., C.L., H.H.R., and J.P. provided reagents/resources, and/or performed experiments, and/or analyzed data; D.A.P., J.R., and C.A.C.M.v.E. conceived the project, led the study, supervised the work, and wrote the paper.

DECLARATION OF INTERESTS

The authors declare no competing interests.

Received: August 18, 2022
Revised: December 31, 2022
Accepted: March 30, 2023
Published: April 25, 2023

REFERENCES

1. O'Brien, K.L., Wolfson, L.J., Watt, J.P., Henkle, E., Deloria-Knoll, M., McCall, N., Lee, E., Mulholland, K., Levine, O.S., Cherian, T., et al. (2009). Burden of disease caused by *Streptococcus pneumoniae* in children younger than 5 years: global estimates. Lancet *374*, 893–902.
2. Adams, W., Bhowmick, R., Bou Ghanem, E.N.B., Wade, K., Shchepetov, M., Weiser, J.N., McCormick, B.A., Tweten, R.K., and Leong, J.M. (2020). Pneumolysin induces 12-lipoxygenase-dependent neutrophil migration during *Streptococcus pneumoniae* infection. J. Immunol. *204*, 101–111.
3. Backhaus, E., Berg, S., Andersson, R., Ockborn, G., Malmström, P., Dahl, M., Nasic, S., and Trollfors, B. (2016). Epidemiology of invasive pneumococcal infections: manifestations, incidence and case fatality rate correlated to age, gender and risk factors. BMC Infect. Dis. *16*, 367.
4. Bentley, S.D., Aanensen, D.M., Mavroidi, A., Saunders, D., Rabbinowitsch, E., Collins, M., Donohoe, K., Harris, D., Murphy, L., Quail, M.A., et al. (2006). Genetic analysis of the capsular biosynthetic locus from all 90 pneumococcal serotypes. PLoS Genet. *2*, e31.
5. García-Suárez, M., Cima-Cabal, M.D., Flórez, N., García, P., Cernuda-Cernuda, R., Astudillo, A., Vázquez, F., De los Toyos, J.R., and Méndez,

F.J. (2004). Protection against pneumococcal pneumonia in mice by monoclonal antibodies to pneumolysin. Infect. Immun. *72*, 4534–4540.

6. Kaur, R., Surendran, N., Ochs, M., and Pichichero, M.E. (2014). Human antibodies to PhtD, PcpA, and Ply reduce adherence to human lung epithelial cells and murine nasopharyngeal colonization by *Streptococcus pneumoniae*. Infect. Immun. *82*, 5069–5075.
7. Yahiaoui, R.Y., den Heijer, C.Dj., van Bijnen, E.M.E., Paget, W.J., Pringle, M., Goossens, H., Bruggeman, C.A., Schellevis, F.G., and Stobberingh, E.E.; APRES Study Team (2016). Prevalence and antibiotic resistance of commensal *Streptococcus pneumoniae* in nine European countries. Future Microbiol. *11*, 737–744.
8. van de Garde, M.D.B., van Westen, E., Poelen, M.C.M., Rots, N.Y., and van Els, C.A.C.M. (2019). Prediction and validation of immunogenic domains of pneumococcal proteins recognized by human $CD4^+$ T cells. Infect. Immun. *87*, e00098-19.
9. Weiser, J.N., Ferreira, D.M., and Paton, J.C. (2018). *Streptococcus pneumoniae*: transmission, colonization and invasion. Nat. Rev. Microbiol. *16*, 355–367.
10. Kadioglu, A., Weiser, J.N., Paton, J.C., and Andrew, P.W. (2008). The role of *Streptococcus pneumoniae* virulence factors in host respiratory colonization and disease. Nat. Rev. Microbiol. *6*, 288–301.
11. Mitsi, E., Roche, A.M., Reiné, J., Zangari, T., Owugha, J.T., Pennington, S.H., Gritzfeld, J.F., Wright, A.D., Collins, A.M., van Selm, S., et al. (2017). Agglutination by anti-capsular polysaccharide antibody is associated with protection against experimental human pneumococcal carriage. Mucosal Immunol. *10*, 385–394.
12. Trzciński, K., Thompson, C.M., Srivastava, A., Basset, A., Malley, R., and Lipsitch, M. (2008). Protection against nasopharyngeal colonization by *Streptococcus pneumoniae* is mediated by antigen-specific $CD4^+$ T cells. Infect. Immun. *76*, 2678–2684.
13. van Rossum, A.M.C., Lysenko, E.S., and Weiser, J.N. (2005). Host and bacterial factors contributing to the clearance of colonization by *Streptococcus pneumoniae* in a murine model. Infect. Immun. *73*, 7718–7726.
14. Shinefield, H.R., and Black, S. (2000). Efficacy of pneumococcal conjugate vaccines in large scale field trials. Pediatr. Infect. Dis. J. *19*, 394–397.
15. Berman-Rosa, M., O'Donnell, S., Barker, M., and Quach, C. (2020). Efficacy and effectiveness of the PCV-10 and PCV-13 vaccines against invasive pneumococcal disease. Pediatrics *145*, e20190377.
16. Ramos-Sevillano, E., Ercoli, G., and Brown, J.S. (2019). Mechanisms of naturally acquired immunity to *Streptococcus pneumoniae*. Front. Immunol. *10*, 358.
17. Brooks, W.A., Chang, L.J., Sheng, X., and Hopfer, R.; PPR02 Study Team (2015). Safety and immunogenicity of a trivalent recombinant PcpA, PhtD, and PlyD1 pneumococcal protein vaccine in adults, toddlers, and infants: a phase I randomized controlled study. Vaccine *33*, 4610–4617.
18. Kamtchoua, T., Bologa, M., Hopfer, R., Neveu, D., Hu, B., Sheng, X., Corde, N., Pouzet, C., Zimmermann, G., and Gurunathan, S. (2013). Safety and immunogenicity of the pneumococcal pneumolysin derivative PlyD1 in a single-antigen protein vaccine candidate in adults. Vaccine *31*, 327–333.
19. Lagousi, T., Basdeki, P., Routsias, J., and Spoulou, V. (2019). Novel protein-based pneumococcal vaccines: assessing the use of distinct protein fragments instead of full-length proteins as vaccine antigens. Vaccines *7*, 9.
20. Baba, H., Kawamura, I., Kohda, C., Nomura, T., Ito, Y., Kimoto, T., Watanabe, I., Ichiyama, S., and Mitsuyama, M. (2001). Essential role of domain 4 of pneumolysin from *Streptococcus pneumoniae* in cytolytic activity as determined by truncated proteins. Biochem. Biophys. Res. Commun. *281*, 37–44.
21. Heuck, A.P., Moe, P.C., and Johnson, B.B. (2010). The cholesterol-dependent cytolysin family of Gram-positive bacterial toxins. Subcell. Biochem. *51*, 551–577.
22. Marshall, J.E., Faraj, B.H., Gingras, A.R., Lonnen, R., Sheikh, M.A., El-Mezgueldi, M., Moody, P.C., Andrew, P.W., and Wallis, R. (2015). The crystal structure of pneumolysin at 2.0 Å resolution reveals the molecular packing of the pre-pore complex. Sci. Rep. *5*, 13293.
23. Rossjohn, J., Feil, S.C., McKinstry, W.J., Tweten, R.K., and Parker, M.W. (1997). Structure of a cholesterol-binding, thiol-activated cytolysin and a model of its membrane form. Cell *89*, 685–692.
24. Vögele, M., Bhaskara, R.M., Mulvihill, E., van Pee, K., Yildiz, Ö., Kühlbrandt, W., Müller, D.J., and Hummer, G. (2019). Membrane perforation by the pore-forming toxin pneumolysin. Proc. Natl. Acad. Sci. USA *116*, 13352–13357.
25. Gilbert, R.J., Jiménez, J.L., Chen, S., Tickle, I.J., Rossjohn, J., Parker, M., Andrew, P.W., and Saibil, H.R. (1999). Two structural transitions in membrane pore formation by pneumolysin, the pore-forming toxin of *Streptococcus pneumoniae*. Cell *97*, 647–655.
26. Lawrence, S.L., Feil, S.C., Morton, C.J., Farrand, A.J., Mulhern, T.D., Gorman, M.A., Wade, K.R., Tweten, R.K., and Parker, M.W. (2015). Crystal structure of *Streptococcus pneumoniae* pneumolysin provides key insights into early steps of pore formation. Sci. Rep. *5*, 14352.
27. Shatursky, O., Heuck, A.P., Shepard, L.A., Rossjohn, J., Parker, M.W., Johnson, A.E., and Tweten, R.K. (1999). The mechanism of membrane insertion for a cholesterol-dependent cytolysin: a novel paradigm for pore-forming toxins. Cell *99*, 293–299.
28. Shepard, L.A., Heuck, A.P., Hamman, B.D., Rossjohn, J., Parker, M.W., Ryan, K.R., Johnson, A.E., and Tweten, R.K. (1998). Identification of a membrane-spanning domain of the thiol-activated pore-forming toxin *Clostridium perfringens* perfringolysin O: an α-helical to β-sheet transition identified by fluorescence spectroscopy. Biochemistry *37*, 14563–14574.
29. Ali, Y.M., Kenawy, H.I., Muhammad, A., Sim, R.B., Andrew, P.W., and Schwaeble, W.J. (2013). Human L-ficolin, a recognition molecule of the lectin activation pathway of complement, activates complement by binding to pneumolysin, the major toxin of *Streptococcus pneumoniae*. PLoS One *8*, e82583.
30. Subramanian, K., Neill, D.R., Malak, H.A., Spelmink, L., Khandaker, S., Dalla Libera Marchiori, G., Dearing, E., Kirby, A., Yang, M., Achour, A., et al. (2019). Pneumolysin binds to the mannose receptor C type 1 (MRC-1) leading to anti-inflammatory responses and enhanced pneumococcal survival. Nat. Microbiol. *4*, 62–70.
31. McNeela, E.A., Burke, A., Neill, D.R., Baxter, C., Fernandes, V.E., Ferreira, D., Smeaton, S., El-Rachkidy, R., McLoughlin, R.M., Mori, A., et al. (2010). Pneumolysin activates the NLRP3 inflammasome and promotes proinflammatory cytokines independently of TLR4. PLoS Pathog. *6*, e1001191.
32. Pichichero, M.E., Kaur, R., Casey, J.R., Xu, Q., Almudevar, A., and Ochs, M. (2012). Antibody response to *Streptococcus pneumoniae* proteins PhtD, LytB, PcpA, PhtE and Ply after nasopharyngeal colonization and acute otitis media in children. Hum. Vaccin. Immunother. *8*, 799–805.
33. Salha, D., Szeto, J., Myers, L., Claus, C., Sheung, A., Tang, M., Ljutic, B., Hanwell, D., Ogilvie, K., Ming, M., et al. (2012). Neutralizing antibodies elicited by a novel detoxified pneumolysin derivative, PlyD1, provide protection against both pneumococcal infection and lung injury. Infect. Immun. *80*, 2212–2220.
34. van Westen, E., Poelen, M.C.M., van den Dobbelsteen, G.P.J.M., Oloo, E.O., Ochs, M.M., Rots, N.Y., and van Els, C.A.C.M. (2018). Immunodominance in T cell responses elicited against different domains of detoxified pneumolysin PlyD1. PLoS One *13*, e0193650.
35. Kuipers, K., Jong, W.S.P., van der Gaast-de Jongh, C.E., Houben, D., van Opzeeland, F., Simonetti, E., van Selm, S., de Groot, R., Koenders, M.I., Azarian, T., et al. (2017). Th17-mediated cross protection against pneumococcal carriage by vaccination with a variable antigen. Infect. Immun. *85*, e00281-17.
36. Voß, F., Kohler, T.P., Meyer, T., Abdullah, M.R., van Opzeeland, F.J., Saleh, M., Michalik, S., van Selm, S., Schmidt, F., de Jonge, M.I., and Hammerschmidt, S. (2018). Intranasal vaccination with lipoproteins confers protection against pneumococcal colonisation. Front. Immunol. *9*, 2405.
37. Wang, Y., Jiang, B., Guo, Y., Li, W., Tian, Y., Sonnenberg, G.F., Weiser, J.N., Ni, X., and Shen, H. (2017). Cross-protective mucosal immunity

mediated by memory Th17 cells against *Streptococcus pneumoniae* lung infection. Mucosal Immunol. *10*, 250–259.

38. Basset, A., Thompson, C.M., Hollingshead, S.K., Briles, D.E., Ades, E.W., Lipsitch, M., and Malley, R. (2007). Antibody-independent, $CD4^+$ T-cell-dependent protection against pneumococcal colonization elicited by intranasal immunization with purified pneumococcal proteins. Infect. Immun. *75*, 5460–5464.
39. Kadioglu, A., Coward, W., Colston, M.J., Hewitt, C.R., and Andrew, P.W. (2004). CD4 T-lymphocyte interactions with pneumolysin and pneumococci suggest a crucial protective role in the host response to pneumococcal infection. Infect. Immun. *72*, 2689–2697.
40. Gray, C., Ahmed, M.S., Mubarak, A., Kasbekar, A.V., Derbyshire, S., McCormick, M.S., Mughal, M.K., McNamara, P.S., Mitchell, T., and Zhang, Q. (2014). Activation of memory Th17 cells by domain 4 pneumolysin in human nasopharynx-associated lymphoid tissue and its association with pneumococcal carriage. Mucosal Immunol. *7*, 705–717.
41. Lundgren, A., Bhuiyan, T.R., Novak, D., Kaim, J., Reske, A., Lu, Y.J., Qadri, F., and Malley, R. (2012). Characterization of Th17 responses to *Streptococcus pneumoniae* in humans: comparisons between adults and children in a developed and a developing country. Vaccine *30*, 3897–3907.
42. Pope, C., Oliver, E.H., Ma, J., Langton Hewer, C.L., Mitchell, T.J., and Finn, A. (2015). Genetic conjugation of components in two pneumococcal fusion protein vaccines enhances paediatric mucosal immune responses. Vaccine *33*, 1711–1718.
43. Zhang, Q., Bagrade, L., Bernatoniene, J., Clarke, E., Paton, J.C., Mitchell, T.J., Nunez, D.A., and Finn, A. (2007). Low CD4 T cell immunity to pneumolysin is associated with nasopharyngeal carriage of pneumococci in children. J. Infect. Dis. *195*, 1194–1202.
44. Castelli, F.A., Buhot, C., Sanson, A., Zarour, H., Pouvelle-Moratille, S., Nonn, C., Gahery-Ségard, H., Guillet, J.G., Ménez, A., Georges, B., and Maillère, B. (2002). HLA-DP4, the most frequent HLA II molecule, defines a new supertype of peptide-binding specificity. J. Immunol. *169*, 6928–6934.
45. Sidney, J., Steen, A., Moore, C., Ngo, S., Chung, J., Peters, B., and Sette, A. (2010). Five HLA-DP molecules frequently expressed in the worldwide human population share a common HLA supertypic binding specificity. J. Immunol. *184*, 2492–2503.
46. González-Galarza, F.F., Takeshita, L.Y., Santos, E.J., Kempson, F., Maia, M.H., da Silva, A.L., Teles e Silva, A.L., Ghattaoraya, G.S., Alfirevic, A., Jones, A.R., and Middleton, D. (2015). Allele frequency net 2015 update: new features for HLA epitopes, KIR and disease and HLA adverse drug reaction associations. Nucleic Acids Res. *43*, D784–D788.
47. Britanova, O.V., Putintseva, E.V., Shugay, M., Merzlyak, E.M., Turchaninova, M.A., Staroverov, D.B., Bolotin, D.A., Lukyanov, S., Bogdanova, E.A., Mamedov, I.Z., et al. (2014). Age-related decrease in TCR repertoire diversity measured with deep and normalized sequence profiling. J. Immunol. *192*, 2689–2698.
48. Bridgeman, J.S., Sewell, A.K., Miles, J.J., Price, D.A., and Cole, D.K. (2012). Structural and biophysical determinants of $\alpha\beta$ T-cell antigen recognition. Immunology *135*, 9–18.
49. Rossjohn, J., Gras, S., Miles, J.J., Turner, S.J., Godfrey, D.I., and McCluskey, J. (2015). T cell antigen receptor recognition of antigen-presenting molecules. Annu. Rev. Immunol. *33*, 169–200.
50. Clayton, G.M., Wang, Y., Crawford, F., Novikov, A., Wimberly, B.T., Kieft, J.S., Falta, M.T., Bowerman, N.A., Marrack, P., Fontenot, A.P., et al. (2014). Structural basis of chronic beryllium disease: linking allergic hypersensitivity and autoimmunity. Cell *158*, 132–142.
51. Dai, S., Murphy, G.A., Crawford, F., Mack, D.G., Falta, M.T., Marrack, P., Kappler, J.W., and Fontenot, A.P. (2010). Crystal structure of HLA-DP2 and implications for chronic beryllium disease. Proc. Natl. Acad. Sci. USA *107*, 7425–7430.
52. Kusano, S., Kukimoto-Niino, M., Satta, Y., Ohsawa, N., Uchikubo-Kamo, T., Wakiyama, M., Ikeda, M., Terada, T., Yamamoto, K., Nishimura, Y., et al. (2014). Structural basis for the specific recognition of the major antigenic peptide from the Japanese cedar pollen allergen Cry j 1 by HLA-DP5. J. Mol. Biol. *426*, 3016–3027.
53. Billington, S.J., Jost, B.H., and Songer, J.G. (2000). Thiol-activated cytolysins: structure, function and role in pathogenesis. FEMS Microbiol. Lett. *182*, 197–205.
54. Ishizuka, J., Stewart-Jones, G.B., van der Merwe, A., Bell, J.I., McMichael, A.J., and Jones, E.Y. (2008). The structural dynamics and energetics of an immunodominant T cell receptor are programmed by its Vβ domain. Immunity *28*, 171–182.
55. Stewart-Jones, G.B., McMichael, A.J., Bell, J.I., Stuart, D.I., and Jones, E.Y. (2003). A structural basis for immunodominant human T cell receptor recognition. Nat. Immunol. *4*, 657–663.
56. Kjer-Nielsen, L., Clements, C.S., Purcell, A.W., Brooks, A.G., Whisstock, J.C., Burrows, S.R., McCluskey, J., and Rossjohn, J. (2003). A structural basis for the selection of dominant $\alpha\beta$ T cell receptors in antiviral immunity. Immunity *18*, 53–64.
57. Tynan, F.E., Burrows, S.R., Buckle, A.M., Clements, C.S., Borg, N.A., Miles, J.J., Beddoe, T., Whisstock, J.C., Wilce, M.C., Silins, S.L., et al. (2005). T cell receptor recognition of a 'super-bulged' major histocompatibility complex class I-bound peptide. Nat. Immunol. *6*, 1114–1122.
58. Tynan, F.E., Reid, H.H., Kjer-Nielsen, L., Miles, J.J., Wilce, M.C., Kostenko, L., Borg, N.A., Williamson, N.A., Beddoe, T., Purcell, A.W., et al. (2007). A T cell receptor flattens a bulged antigenic peptide presented by a major histocompatibility complex class I molecule. Nat. Immunol. *8*, 268–276.
59. Gras, S., Saulquin, X., Reiser, J.B., Debeaupuis, E., Echasserieau, K., Kissenpfennig, A., Legoux, F., Chouquet, A., Le Gorrec, M., Machillot, P., et al. (2009). Structural bases for the affinity-driven selection of a public TCR against a dominant human cytomegalovirus epitope. J. Immunol. *183*, 430–437.
60. Stewart-Jones, G.B., Simpson, P., van der Merwe, P.A., Easterbrook, P., McMichael, A.J., Rowland-Jones, S.L., Jones, E.Y., and Gillespie, G.M. (2012). Structural features underlying T-cell receptor sensitivity to concealed MHC class I micropolymorphisms. Proc. Natl. Acad. Sci. USA *109*, E3483–E3492.
61. Miles, J.J., Douek, D.C., and Price, D.A. (2011). Bias in the $\alpha\beta$ T-cell repertoire: implications for disease pathogenesis and vaccination. Immunol. Cell Biol. *89*, 375–387.
62. Venturi, V., Price, D.A., Douek, D.C., and Davenport, M.P. (2008). The molecular basis for public T-cell responses? Nat. Rev. Immunol. *8*, 231–238.
63. Solberg, O.D., Mack, S.J., Lancaster, A.K., Single, R.M., Tsai, Y., Sanchez-Mazas, A., and Thomson, G. (2008). Balancing selection and heterogeneity across the classical human leukocyte antigen loci: a meta-analytic review of 497 population studies. Hum. Immunol. *69*, 443–464.
64. Chu, N.D., Bi, H.S., Emerson, R.O., Sherwood, A.M., Birnbaum, M.E., Robins, H.S., and Alm, E.J. (2019). Longitudinal immunosequencing in healthy people reveals persistent T cell receptors rich in highly public receptors. BMC Immunol. *20*, 19.
65. Emerson, R.O., DeWitt, W.S., Vignali, M., Gravley, J., Hu, J.K., Osborne, E.J., Desmarais, C., Klinger, M., Carlson, C.S., Hansen, J.A., et al. (2017). Immunosequencing identifies signatures of cytomegalovirus exposure history and HLA-mediated effects on the T cell repertoire. Nat. Genet. *49*, 659–665.
66. Benati, D., Galperin, M., Lambotte, O., Gras, S., Lim, A., Mukhopadhyay, M., Nouël, A., Campbell, K.A., Lemercier, B., Claireaux, M., et al. (2016). Public T cell receptors confer high-avidity CD4 responses to HIV controllers. J. Clin. Invest. *126*, 2093–2108.
67. Galperin, M., Farenc, C., Mukhopadhyay, M., Jayasinghe, D., Decroos, A., Benati, D., Tan, L.L., Ciacchi, L., Reid, H.H., Rossjohn, J., et al. (2018). $CD4^+$ T cell-mediated HLA class II cross-restriction in HIV controllers. Sci. Immunol. *3*, eaat0687.
68. Corrotte, M., Fernandes, M.C., Tam, C., and Andrews, N.W. (2012). Toxin pores endocytosed during plasma membrane repair traffic into the lumen of MVBs for degradation. Traffic *13*, 483–494.

69. Reynisson, B., Alvarez, B., Paul, S., Peters, B., and Nielsen, M. (2020). NetMHCpan-4.1 and NetMHCIIpan-4.0: improved predictions of MHC antigen presentation by concurrent motif deconvolution and integration of MS MHC eluted ligand data. Nucleic Acids Res. *48*, W449–W454.

70. Mureithi, M.W., Finn, A., Ota, M.O., Zhang, Q., Davenport, V., Mitchell, T.J., Williams, N.A., Adegbola, R.A., and Heyderman, R.S. (2009). T cell memory response to pneumococcal protein antigens in an area of high pneumococcal carriage and disease. J. Infect. Dis. *200*, 783–793.

71. Kabsch, W. (2010). XDS. Acta Crystallogr. D Biol. Crystallogr. *66*, 125–132.

72. Winn, M.D., Ballard, C.C., Cowtan, K.D., Dodson, E.J., Emsley, P., Evans, P.R., Keegan, R.M., Krissinel, E.B., Leslie, A.G., McCoy, A., et al. (2011). Overview of the CCP4 suite and current developments. Acta Crystallogr. D Biol. Crystallogr. *67*, 235–242.

73. Adams, P.D., Afonine, P.V., Bunkóczi, G., Chen, V.B., Davis, I.W., Echols, N., Headd, J.J., Hung, L.W., Kapral, G.J., Grosse-Kunstleve, R.W., et al. (2010). Phenix: a comprehensive Python-based system for macromolecular structure solution. Acta Crystallogr. D Biol. Crystallogr. *66*, 213–221.

74. Emsley, P., Lohkamp, B., Scott, W.G., and Cowtan, K. (2010). Features and development of coot. Acta Crystallogr. D Biol. Crystallogr. *66*, 486–501.

75. Cowieson, N.P., Aragao, D., Clift, M., Ericsson, D.J., Gee, C., Harrop, S.J., Mudie, N., Panjikar, S., Price, J.R., Riboldi-Tunnicliffe, A., et al. (2015). MX1: a bending-magnet crystallography beamline serving both chemical and macromolecular crystallography communities at the Australian Synchrotron. J. Synchrotron Radiat. *22*, 187–190.

76. Aragão, D., Aishima, J., Cherukuvada, H., Clarken, R., Clift, M., Cowieson, N.P., Ericsson, D.J., Gee, C.L., Macedo, S., Mudie, N., et al. (2018). MX2: a high-flux undulator microfocus beamline serving both the chemical and macromolecular crystallography communities at the Australian Synchrotron. J. Synchrotron Radiat. *25*, 885–891.

77. Mamedov, I.Z., Britanova, O.V., Bolotin, D.A., Chkalina, A.V., Staroverov, D.B., Zvyagin, I.V., Kotlobay, A.A., Turchaninova, M.A., Fedorenko, D.A., Novik, A.A., et al. (2011). Quantitative tracking of T cell clones after haematopoietic stem cell transplantation. EMBO Mol. Med. *3*, 201–207.

78. Wang, G.C., Dash, P., McCullers, J.A., Doherty, P.C., and Thomas, P.G. (2012). T cell receptor αβ diversity inversely correlates with pathogen-specific antibody levels in human cytomegalovirus infection. Sci. Transl. Med. *4*, 128ra42.

79. Boulter, J.M., Glick, M., Todorov, P.T., Baston, E., Sami, M., Rizkallah, P., and Jakobsen, B.K. (2003). Stable, soluble T-cell receptor molecules for crystallization and therapeutics. Protein Eng. *16*, 707–711.

80. Clements, C.S., Kjer-Nielsen, L., MacDonald, W.A., Brooks, A.G., Purcell, A.W., McCluskey, J., and Rossjohn, J. (2002). The production, purification and crystallization of a soluble heterodimeric form of a highly selected T-cell receptor in its unliganded and liganded state. Acta Crystallogr. D Biol. Crystallogr. *58*, 2131–2134.

81. Broughton, S.E., Petersen, J., Theodossis, A., Scally, S.W., Loh, K.L., Thompson, A., van Bergen, J., Kooy-Winkelaar, Y., Henderson, K.N., Beddoe, T., et al. (2012). Biased T cell receptor usage directed against human leukocyte antigen DQ8-restricted gliadin peptides is associated with celiac disease. Immunity *37*, 611–621.

82. Henderson, K.N., Reid, H.H., Borg, N.A., Broughton, S.E., Huyton, T., Anderson, R.P., McCluskey, J., and Rossjohn, J. (2007). The production and crystallization of the human leukocyte antigen class II molecules HLA-DQ2 and HLA-DQ8 complexed with deamidated gliadin peptides implicated in coeliac disease. Acta Crystallogr. Sect. F Struct. Biol. Cryst. Commun. *63*, 1021–1025.

83. Petersen, J., Montserrat, V., Mujico, J.R., Loh, K.L., Beringer, D.X., Van Lummel, M., Thompson, A., Mearin, M.L., Schweizer, J., Kooy-Winkelaar, Y., et al. (2014). T-cell receptor recognition of HLA-DQ2–gliadin complexes associated with celiac disease. Nat. Struct. Mol. Biol. *21*, 480–488.

84. Lefranc, M.P., Giudicelli, V., Kaas, Q., Duprat, E., Jabado-Michaloud, J., Scaviner, D., Ginestoux, C., Clément, O., Chaume, D., and Lefranc, G. (2005). IMGT, the international ImMunoGeneTics information system. Nucleic Acids Res. *33*, D593–D597.

STAR★METHODS

KEY RESOURCES TABLE

REAGENT or RESOURCE	SOURCE	IDENTIFIER
Antibodies		
Anti-CD3–Alexa Fluor 700	BioLegend	Cat# 317340; RRID: AB_2563408
Anti-CD4–BV711	BioLegend	Cat# 317440; RRID: AB_2562912
Anti-CD8–BV785	BioLegend	Cat# 344740; RRID: AB_2566202
Anti-CD14–APC-Cy7	BioLegend	Cat# 325620; RRID: AB_830693
Anti-CD19–APC-Cy7	BioLegend	Cat# 363010; RRID: AB_2564193
Anti-CD25–BUV737	BD Biosciences	Cat# 612807; RRID: AB_2916878
Anti-HLA-DP (clone B7/21)	Leinco Technologies	Cat# H266; RRID: AB_2892891
Anti-HLA-DQ (clone SPV-L3)	Thermo Fisher Scientific	Cat# NBP24504101; RRID: N/A
Anti-HLA-DR (clone B8.11-2)	In-house (RIVM)	N/A
Anti-CCR7–BV421	BioLegend	Cat# 353208; RRID: AB_11203894
Anti-CD3–APC-Fire750	BioLegend	Cat# 344840; RRID: AB_2572114
Anti-CD4–FITC	Thermo Fisher Scientific	Cat# MHCD0401; RRID: AB_10392546
Anti-CD8–BV711	BioLegend	Cat# 301044; RRID: AB_2562906
Anti-CD14–V500	BD Horizon	Cat# 561391; RRID: AB_10611856
Anti-CD19–V500	BD Horizon	Cat# 561121; RRID: AB_10562391
Anti-CD45RA–ECD	Beckman Coulter	Cat# IM2711U; RRID: AB_10640553
Bacterial and virus strains		
Streptococcus pneumoniae TIGR4 ΔCPS	Radboud University Medical Center	N/A
Listeria monocytogenes	RIVM Reference Laboratory Strain Collection F	N/A
Streptococcus parasanguines	RIVM Reference Laboratory Strain Collection F	N/A
Escherichia coli BL21-DE3	Thermo Fisher Scientific	Cat# EC0114
Biological samples		
Human PBMCs	This study	N/A
FCS	Greiner Bio-One	Cat# 758093
Human AB serum	Sigma-Aldrich	Cat# H6914
HLA-genotyped EBV-transformed B-LCLs	This study	N/A
Chemicals, peptides, and recombinant proteins		
LymphoPrep	Sanbio	Cat# 1858-6
DMSO	Sigma-Aldrich	Cat# 276855

(*Continued on next page*)

Continued

REAGENT or RESOURCE	SOURCE	IDENTIFIER
Detoxified pneumolysin	Sanofi Pasteur	N/A
Pneumolysin	Sanofi Pasteur	N/A
Brain-Heart-Infusion Broth	Tritium Microbiologie	Cat# B455.24.0005
AIM-V Medium	Thermo Fisher Scientific	Cat# 12055091
CellTrace Violet	Thermo Fisher Scientific	Cat# C34557
Penicillin/streptomycin	Thermo Fisher Scientific	Cat# 15140122
IMDM	Thermo Fisher Scientific	Cat# 12440053
Zombie NIR	BioLegend	Cat# 423106
Tetramer–PE HLA-DP*02/ECT	NIH Tetramer Core Facility	N/A
Tetramer–PE HLA-DP*04/ECT	NIH Tetramer Core Facility	N/A
Phytohemagglutinin	Sigma-Aldrich	Cat# 11249738001
Human IL-4	PeproTech	Cat# 200-04
Human GM-CSF	PeproTech	Cat# 300-23
LIVE/DEAD Fixable Aqua	Thermo Fisher Scientific	Cat# L34957
SuperScript II Reverse Transcriptase	Thermo Fisher Scientific	Cat# 18064014
Q5 High-Fidelity DNA Polymerase	New England Biolabs	Cat# M0491L
Paraformaldehyde	Sigma-Aldrich	Cat# 8.18715
Superscript Vilo cDNA Synthesis Kit	Thermo Fisher Scientific	Cat# 11754050
DEAE-cellulose	Sigma-Aldrich	Cat# 30477
HiTrap Phenyl Sepharose HP	Cytiva	Cat# 17519501
HiTrap Q HP	GE Healthcare	Cat# 17115401
Ni Sepharose 6 Fast-Flow	GE Healthcare	Cat# 17531802
Enterokinase	New England Biolabs	Cat# P8070L
PEG 3350	Sigma-Aldrich	Cat# PHR2362
Recombinant listeriolysin (LLO) protein	Abcam	Cat# ab83345
Recombinant perfringolysin (PFO) protein	Cusabio	Cat# CSB-EP314820CMB
Recombinant streptolysin O (SLO) protein	Abcam	Cat# ab63978
Synthetic peptides representing Ply	Table S7	N/A
Critical commercial assays		
LEGENDplex Human T Helper Cytokine Panels V2	BioLegend	Cat# 741028
Deposited data		
HLA-DP4-Ply$_{427–441}$	Protein Data Bank	PDB: 7T2A
5F-HLA-DP4-Ply$_{427–441}$	Protein Data Bank	PDB: 7T2B
B5-HLA-DP4-Ply$_{427–441}$	Protein Data Bank	PDB: 7T2C
B1-HLA-DP4-Ply$_{427–441}$	Protein Data Bank	PDB: 7T2D
Experimental models: Cell lines		
BTI-TN-5B1-4 (Hi Five)	Thermo Fisher Scientific	Cat# B85502
IPLB-Sf21-AE (Sf9)	Thermo Fisher Scientific	Cat# B82501
Oligonucleotides		
Primers used to sequence clonal TCRs	Table S8	N/A
Software and algorithms		
FlowJo software version 10	FlowJo LLC	N/A
BIAevaluation version 3.1	Biacore AB	N/A
GraphPad Prism version 8.0	GraphPad	N/A
XDS	Kabsch[71]	N/A
SCALA or AIMLESS in the CCP4 suite	Winn et al.[72]	N/A
Phaser in the PHENIX suite	Adams et al.[73]	N/A
Coot	Emsley et al.[74]	N/A

(*Continued on next page*)

Continued

REAGENT or RESOURCE	SOURCE	IDENTIFIER
Other		
Anti-PE UltraPure MicroBeads	Miltenyi Biotec	Cat# 130-105-639
RNeasy Micro Kit	Qiagen	Cat# 74004
PCR Clean Up Kit	Macherey-Nagel	Cat# 740609.50
HiSeq 2500 System	Illumina	N/A
Cogent M1 TFF System	Merck Millipore	N/A
BIAcore T200 instrument	GE Healthcare	N/A
ADSC Quantum 210r detector	Cowieson et al.[75]	N/A
EIGER X 16M pixel detectors at 100 K	Aragão et al.[76]	N/A
Superdex S200 16/600	GE Healthcare	Cat# GE28-9893-35
Superdex S200 10/300	GE Healthcare	Cat# GE17-5175-01
MicroBeta Counter	Perkin Elmer	N/A

RESOURCE AVAILABILITY

Lead contact

Further information and requests for resources and reagents should be directed to and will be fulfilled by the lead contact, Cécile van Els (cecile.van.els@rivm.nl).

Materials availability

Plasmids generated during this study are available upon reasonable request subject to institutional legislation.

Data and code availability

The published article includes all data generated during this study and does not describe new code.

EXPERIMENTAL MODEL AND SUBJECT DETAILS

Donors and ethics

Healthy adult donors were recruited from the Dutch Blood Bank via a Not-For-Transfusion Study (NVT0201.01, Sanquin). Donors with clinically symptomatic and laboratory-confirmed *S. pneumoniae* infection were recruited via the IMMfact Study (NL46795.094.13), initially approved and managed by the METC Noord-Holland (Alkmaar, The Netherlands) and subsequently approved and managed by the METC MEC-U (Utrecht, The Netherlands). Data were generated from a total of 59 healthy adult donors (28 female, 30 male, 1 unknown) with a median age of 44 years (range, 22–64 years). Six donors with available material were selected from the IMMfact Study (Table S1). All donors and parents/guardians of minor participants provided written informed consent in accordance with the principles of the Declaration of Helsinki.

Samples

Venous blood samples from healthy adult donors were collected into citrate-anti-coagulated blood bags (500 mL). Serial venous blood samples from IMMfact donors were collected into sodium heparin tubes (9 mL) during house visits within 3 months and at 9 ± 1, 18 ± 2, and/or 36 ± 3 months after symptomatic infection with *S. pneumoniae*. PBMCs were isolated via density gradient centrifugation over LymphoPrep (Sanbio) and cryopreserved in fetal calf serum (FCS, Greiner Bio-One) containing 10% dimethyl sulfoxide (DMSO, Sigma-Aldrich).

Synthetic peptides, proteins, and bacterial strains

Peptides with a maximum length of 18 amino acids were purchased commercially (Pepscan) and dissolved in DMSO at a stock concentration of 1 mM (Table S7). Purified wildtype Ply and dPly, genetically mutated at T65C, G293C, and C428A, were kindly provided by M. Ochs (Sanofi Pasteur). All purified CDCs, including LLO (Abcam), PFO (Cusabio), and SLO (Abcam), were heat-inactivated before use for 15 min at 80°C. TIGR4$_{\Delta CPS}$ was kindly provided by M. de Jonge (Radboud University Medical Center) and subsequently cultured up to an optical density of 0.6. Clinical isolates of *L. monocytogenes* and *S. parasanguines* were kindly provided by Frans Reubsaet from the RIVM Reference Laboratory Strain Collection and subsequently cultured overnight in Brain-Heart-Infusion Broth (Tritium Microbiologie). Whole cell preparations were generated by heat-inactivating the biomass for 1 h at 56°C (*S. pneumoniae* and *S. parasanguines*) or 80°C (*L. monocytogenes*).

METHOD DETAILS

HLA genotyping

DNA was isolated from PBMCs at the Laboratory of Translational Immunology, University Medical Center Utrecht. Four-digit genotyping for HLA class II DPA1 and DPB1 was performed using sequence-specific oligonucleotide PCRs in conjunction with Luminex.

Cell proliferation assays

For the ^{3}HTdr incorporation assay, PBMCs were resuspended in AIM-V medium (Thermo Fisher Scientific) containing 2% human AB serum (Sigma-Aldrich) and dispensed into 96-well U-bottom plates at 1.5×10^{5} cells/well in the presence of medium alone (negative control), individual or pooled peptides (1 μM), or protein (1 μg/mL). Stimulations were performed in triplicate or quadruplicate for 5 days at 37°C with 5% CO_2. Proliferation was determined by adding ^{3}HTdr (18 kBq/well) and incubating the cells overnight at 37°C with 5% CO_2. Cells were harvested onto a filter, and incorporated label was determined as counts per minute (cpm) using a MicroBeta Counter (Perkin Elmer). The mean cpm from stimulated wells was divided by the mean cpm from negative control wells to determine the SI. Positive responses were assigned at SI values $\geq$2. For the flow cytometric dye dilution assay, PBMCs were labeled with CellTrace Violet according to the manufacturer's instructions (Thermo Fisher Scientific). Cells were stimulated as described above for 7 days at 37°C with 5% CO_2. After incubation, cells were pooled from duplicate wells and stained with Zombie NIR (BioLegend), tetramer–PE (NIH Tetramer Core Facility), and the following directly conjugated monoclonal antibodies: (i) anti-CD3–Alexa Fluor 700 (clone SK7), anti-CD4–BV711 (clone OKT4), anti-CD8–BV785 (clone SK1), anti-CD14–APC-Cy7 (clone 63D3), and anti-CD19–APC-Cy7 (clone HIB19) from BioLegend; and (ii) anti-CD25–BUV737 (clone 2A3) from BD Biosciences. Cells were acquired using an LSRFortessa (BD Biosciences), and data were analyzed using FlowJo software version 10 (FlowJo LLC).

Cytokine secretion

Cytokines were measured in culture supernatants using a multiplex bead-based assay (LEGENDplex Human Th Panel) that quantifies IL-2, IL-4, IL-5, IL-6, IL-9, IL-10, IL-13, IL-17A, IL-17F, IL-21, IL-22, IFN-γ, and TNF-α (BioLegend). Data were acquired using a FACSCanto (BD Biosciences).

Generation of CD4^{+} T cell clones

PBMCs were stimulated with dPly (1 μg/mL) in AIM-V medium (Thermo Fisher Scientific) containing 2% human AB serum (Sigma-Aldrich) for 7 days at 37°C with 5% CO_2. Cells were then subjected to limiting dilution, dispensed into 96-well U-bottom plates containing 1.5×10^{5} γ-irradiated feeder PBMCs/well, and stimulated with phytohemagglutinin (1 μg/mL) for 2–3 weeks at 37°C with 5% CO_2. Expanding cultures from plates with <36% cell outgrowth were evaluated for reactivity to whole protein stimulation in the presence of autologous moDCs. Responsive clones were stimulated with peptides to assess epitope specificity.

Restriction analysis of CD4^{+} T cell clones

HLA restriction was assessed by measuring proliferation in response to stimulation with dPly-loaded autologous or HLA-genotyped EBV-transformed B-LCLs. Briefly, B-LCLs were mock pulsed or pulsed with dPly (1 μg/mL) overnight at 37°C with 5% CO_2, washed in phosphate-buffered saline (PBS), fixed with 0.25% paraformaldehyde for 10 min at room temperature, and washed again in 0.2 M glycine. The restriction element was confirmed using anti-HLA-DP (clone B7/21, Leinco Technologies), anti-HLA-DQ (clone SPV-L3, Thermo Fisher Scientific), or anti-HLA-DR (clone B8.11-2, RIVM).

Generation of monocyte-derived dendritic cells

PBMCs were resuspended in IMDM (Thermo Fisher Scientific) containing 1% FCS and 1% penicillin/streptomycin (Thermo Fisher Scientific), dispensed into T75 flasks at 40×10^{6} cells/flask, and incubated for 2 h at 37°C with 5% CO_2. Monocytes were isolated via plastic adherence. Adherent cells were washed once in prewarmed PBS and differentiated in IMDM containing 1% FCS, 1% penicillin/streptomycin, 50 U/mL IL-4 (PeproTech), and 500 U/mL GM-CSF (PeproTech) for 5 days at 37°C with 5% CO_2.

Tetramer staining

PE-labeled DPB1*02:01/DPA1*01:03 *S. pneumoniae* $Ply_{427–439}$ ECTGLAWEWWRTV (HLA-DP*02/ECT) and DPB1*04:01/DPA1*01:03 *S. pneumoniae* $Ply_{427–439}$ ECTGLAWEWWRTV (HLA-DP*04/ECT) tetramers were provided by the NIH Tetramer Core Facility. Cells were stained for 45 min at room temperature in the dark with each tetramer prediluted 1:200 in FACS buffer (PBS containing 0.5% bovine serum albumin).

Cell sorting

PBMCs were stained with the PE-labeled DP*04/ECT tetramer and magnetically enriched using anti-PE UltraPure MicroBeads (Miltenyi Biotec). Cells were then stained with LIVE/DEAD Fixable Aqua (Thermo Fisher Scientific) and the following directly conjugated monoclonal antibodies: (i) anti-CD3–APC-Fire750 (clone SK7), anti-CD8–BV711 (clone RPA-T8), and anti-CCR7–BV421 (clone GO43H7) from BioLegend; (ii) anti-CD14–V500 (clone H5E2) and anti-CD19–V500 (clone HIB19) from BD Biosciences; (iii) anti-

CD4–FITC (clone S3.5) from Thermo Fisher Scientific; and (iv) anti-CD45RA–ECD (clone 2H4LDH11LDB9) from Beckman Coulter. Viable tetramer$^+$CD3$^+$CD4$^+$CD8$^-$CD14$^-$CD19$^-$ cells were index-sorted directly into 96-well V-bottom plates at 1 cell/well using a custom-modified FACSAria II (BD Biosciences).

TCR sequencing of T cell clones

T cell clones were sequenced essentially as described previously.[77] Briefly, RNA was isolated using an RNeasy Micro Kit (Qiagen), and cDNA was synthesized via template-switch using SuperScript II Reverse Transcriptase (Thermo Fisher Scientific) with 5' switch adaptors incorporating unique molecular identifiers and primers AC1R (ACACATCAGAATCCTTACTTTG) and BC1R (CAGTATCT GGAGTCATTGA). Products were purified using a PCR Clean Up Kit (Macherey-Nagel). cDNA was amplified using Q5 High-Fidelity DNA Polymerase (New England Biolabs) with primers AC2R (TACACGGCAGGGTCAGGGT) and BC2R (TGCTTCTGATG GCTCAAACAC). Thermocycling parameters were 5 min at 95°C, followed by 25 cycles of 20 s at 95°C, 20 s at 65°C, and 1 min at 72°C, with a final extension for 5 min at 72°C. Amplicons were purified using a PCR Clean Up Kit (Macherey-Nagel). A second amplification over 20 cycles under otherwise identical conditions was then performed separately for TRA and TRB using primers Hum_ACJ ((N)2–4(XXXXX)ACACSTTKTTCAGGTCCTC) and Hum_BCJ ((N)2–4(XXXXX)GGGTCAGGGTTCTGGATAT). Amplicons were visualized on a 1% agarose gel and purified using a Nucleospin Gel and PCR Clean Up Kit (Macherey-Nagel). TCR sequencing was performed using a paired-end (2 × 250 bp) strategy with a HiSeq 2500 System (Illumina).

TCR sequencing of single T cells

T cells sorted directly *ex vivo* were sequenced essentially as described previously.[78] Briefly, cDNA was synthesized from single-cell RNA templates using a Superscript Vilo cDNA Synthesis Kit (Thermo Fisher Scientific), and products were amplified separately using a multiplex PCR with nested primers for TRA or TRB. Primer sequences are listed in the original publication.[78] Amplicons were visualized on a 2% agarose gel and purified using a Nucleospin Gel and PCR Clean Up Kit (Macherey-Nagel). TCR sequencing was performed using reverse primers for TRAC or TRBC (Genewiz).

Protein expression and purification

The extracellular domains of the TCR α- and β-chains were engineered with an interchain disulfide bond and expressed in *E. coli* BL21-DE3 cells (Thermo Fisher Scientific). Heterodimers were refolded at an equimolar α:β ratio for 3 days at 4°C and dialyzed in 10 mM Tris-HCl pH 8. TCRs were purified using immobilized DEAE-cellulose (Sigma-Aldrich), size exclusion (Superdex S200 16/600, GE Healthcare), hydrophobic interaction (HiTrap Phenyl Sepharose HP, Cytiva), and anion exchange (HiTrap Q HP, GE Healthcare) chromatography.[79,80] The extracellular domains of HLA-DP were produced in *Trichoplusia ni* BTI-TN-5B1-4 (Hi Five) cells (Thermo Fisher Scientific) using a baculovirus expression system as described previously.[81–83] Briefly, the baculovirus HLA-DP expression construct contained a C-terminal enterokinase-cleavable Fos/Jun leucine zipper to allow for correct dimerization, and the C-terminus of the β-chain was further engineered to encode a BirA ligase recognition sequence for biotinylation and a polyhistidine tag for purification. The extracellular domains of the HLA-DP2/DP4 (DPA1*01:03 and DPB1*02:01/DPB1*04:01) α- and β-chains with the pneumolysin epitope ($Ply_{427–441}$ with mutations E427G and C428A) or the control oxytocinase peptide EKKYFAATQFAPLAAR ($Oxy_{271–286}$ with mutation E281A) attached covalently were concentrated and diafiltrated from supernatants in 10 mM Tris-HCl pH 8, 500 mM NaCl using a Cogent M1 TFF System (Merck Millipore) and then purified via immobilized metal ion affinity (Ni Sepharose 6 Fast-Flow, GE Healthcare) and size exclusion (Superdex S200 16/600, GE Healthcare) chromatography. The leucine zipper and associated tags were cleaved using enterokinase (New England Biolabs). All complexes were then purified again using anion exchange (HiTrap Q HP, GE Healthcare) chromatography. For crystallization trials, HLA-DP4-$Ply_{427–441}$ was mixed at a 1:1 ratio with each TCR, and the resulting complexes were purified via gel filtration (Superdex S200 10/300, GE Healthcare).

Surface plasmon resonance

SPR experiments were conducted at 25°C on a BIAcore T200 instrument (GE Healthcare) with TBS-P buffer (10 mM Tris-HCl pH 8, 150 mM NaCl, 0.005% surfactant P20). Biotinylated HLA-DP4-$Ply_{427–441}$, HLA-DP2-$Ply_{427–441}$, and HLA-DP4-$Oxy_{271–286}$ were immobilized on a research-grade streptavidin chip at an average of ~2,000–4,000 response units per complex. A mouse H_2D^b complex was immobilized for reference. Experiments were conducted with serial dilutions of each TCR starting at a concentration of 200 μM. The flow rate was 30 μL/min. Two independent experiments with two replicates were performed for each TCR. Data were plotted using the 1:1 Langmuir binding model in BIAevaluation version 3.1 and Prism version 8.0.0 (GraphPad) (Table 1; Figures S3 and S4).

Crystallization and data collection

Crystals were grown using the hanging-drop vapor-diffusion method at 20°C by mixing equal volumes of protein in 10 mM Tris-HCl pH 8, 150 mM NaCl with mother liquor solution at a ratio of 1:1. Crystals of the HLA-DP4-$Ply_{427–441}$ binary complex formed at a concentration of ~8 mg/mL in 0.15–0.2 M NaCl, 20–23% PEG 3350. Crystals of the public B1-HLA-DP4-$Ply_{427–441}$ ternary complex formed at a concentration of ~15–18 mg/mL in 1.5–1.65 M K Na tartrate, 0.05–0.2 M Tris-HCl pH 8. Crystals of the private 5F-HLA-DP4-$Ply_{427–441}$ ternary complex formed at a concentration of ~10–12 mg/mL in 8–12% Tacsimate pH 8, 20–25% PEG 3350. Crystals of the private B5-HLA-DP4-$Ply_{427–441}$ ternary complex formed at a concentration of ~15–18 mg/mL in mother liquor solution comprising 0.1–0.2 M Ca acetate, 0.1 M Tris-HCl pH 8.5, 10–20% PEG 3350. Crystals were cryoprotected before flash freezing in

liquid nitrogen via gradual transfer into mother liquor solution supplemented with 20% glycerol for the HLA-DP4-Ply$_{427–441}$ binary complex, 20% Tacsimate pH 8 for the B1-HLA-DP4-Ply$_{427–441}$ ternary complex, and 20% ethylene glycol for the 5F-HLA-DP4-Ply$_{427–441}$ and B5-HLA-DP4-Ply$_{427–441}$ ternary complexes. Data were collected on the MX1 and MX2 beamlines at the Australian Synchrotron using the ADSC Quantum 210r detector[75] or EIGER X 16M pixel detectors at 100 K.[76] Data were integrated using XDS[71] and scaled using SCALA or AIMLESS in the CCP4 suite.[72]

Structure determination, refinement, and validation

Crystal structures were solved by molecular replacement using Phaser in the PHENIX suite.[73] The search model for HLA-DP4-Ply$_{427–441}$ was HLA-DP2 (PDB ID, 4P5K). The refined HLA-DP4-Ply$_{427–441}$ structure was then used to model each ternary complex, together with the BC8B TCR (PDB ID, 6CUH) for the 5F TCR, the S2 TCR (PDB ID, 4OZI) for the B5 TCR, and the HY.1B11 TCR (PDB ID, 4MAY) for the B1 TCR. The structures were refined by iterative rounds of manual adjustment in Coot[74] and restrained refinement in PHENIX.[73] The TCR variable domains were numbered according to the IMGT unique numbering system,[84] with the exception of two residues in the CDR3β loop of the B5 TCR, which were labeled as 112A and 113A. Data processing and refinement statistics for all complexes are summarized in Table S3.

Accession numbers

The coordinates and structure factors for HLA-DP4-Ply$_{427–441}$, 5F-HLA-DP4-Ply$_{427–441}$, B5-HLA-DP4-Ply$_{427–441}$, and B1-HLA-DP4-Ply$_{427–441}$ have been deposited in the Protein Data Bank under entry codes PDB: 7T2A, PDB: 7T2B, PDB: 7T2C, and PDB: 7T2D, respectively.

QUANTIFICATION AND STATISTICAL ANALYSIS

Statistics

Differences among groups were compared using one-way analysis of variance (ANOVA) with Tukey's post-hoc test or the Kruskal-Wallis test with Dunn's post-hoc test in Prism version 9.3.1 (GraphPad). Significance was assigned at p values below 0.05.